China Geology 8 (2025) 58−76

China Geology

Journal homepage: http://chinageology.cgs.cn
https://www.sciencedirect.com/journal/china-geology

Carboniferous-Early Permian heterogeneous distribution of porous carbonate reservoirs in the Central Uplift of the South Yellow Sea Basin and its hydrocarbon potential analysis

Shu-yu Wu[a, b, c, d, f], Jun Liu[b, e,*], Jian-wen Chen[e, f], Qi-liang Sun[g], Yin-guo Zhang[e, f], Jie Liang[e, f], Yong-cai Feng[b]

[a] *School of Engineering, China University of Geoscience, Wuhan* 430074, *China*
[b] *Yantai Center of Coastal Zone Geological Survey, China Geological Survey, Ministry of Natural Resources, Yantai* 264001, *China*
[c] *Key Laboratory of Submarine Geosicences, Ministry of Natural Resources, Hangzhou* 310012, *China*
[d] *Chinese Academy of Geological Sciences, China Geological Survey, Ministry of Natural Resources, Beijing* 100037, *China*
[e] *Laboratory for Marine Mineral Resources, Qingdao National Laboratory for Marine Science and Technology, Qingdao* 266061, *China*
[f] *The Key Laboratory of Gas Hydrate, Ministry of Natural Resources, Qingdao Institute of Marine Geology, China Geological Survey, Ministry of Natural Resources, Qingdao* 266071, *China*
[g] *College of Marine Science and Technology, China University of Geoscience, Wuhan* 430074, *China*

ARTICLE INFO

Article history:
Received 3 February 2023
Received in revised form 19 September 2023
Accepted 16 October 2023
Available online 25 October 2023

Keywords:
Sedimentary
Heterogeneous porous carbonate reservoirs
C-H-Sr isotope analysis
Carboniferous-Early Permian
Chuanshan Formation
Huanglong Formation
Pre-stack simultaneous inversion technique
Oil-gas exploration engineering
Hydrocarbon accumulation
Hydrocarbon potential
Central Uplift of the South Yellow Sea Basin

ABSTRACT

Mesozoic-Palaeozoic marine carbonate rocks are crucial hydrocarbon reservoirs in the Central Uplift area of the South Yellow Sea Basin (SYSB). Due to the scarcity of boreholes and the significant heterogeneity of carbonate reservoirs, the distribution of porous carbonate reservoirs and their related key controlling factors remain unclear. In this study, factors affecting the distribution of porous Carboniferous-Early Permian carbonate reservoirs in the SYSB were investigated through seismic inversion and isotope analysis. The log-seismic characteristics of porous carbonate reservoirs, sensitive lithology parameters, and physical property parameters were extracted and analyzed. The pre-stack simultaneous inversion technique was applied to predict the lithology and physical properties of porous carbonate reservoirs. Moreover, the sedimentary of carbonate was analyzed using isotopes of carbon, oxygen, and strontium. The results show that porous carbonate reservoirs are mainly developed in the open platform sediments with porosities of 3%–5% and are mainly distributed in the paleo-highland (Huanglong Formation and Chuanshan Formation) and the slope of paleo-highland (Hezhou Formation). The porous carbonate reservoirs of the Qixia Formation are only locally developed. In addition, the negative $\delta^{13}C$ excursions indicate a warm and humid tropical climate with three sea-level fluctuations in the study area from the Carboniferous to Early Permian. The favorable conditions for developing porous carbonate rocks include the sedimentary environment and diagenetic process. The primary pore tends to form in high-energy environments of the paleo-highland, and the secondary pore is increased by dissolution during the syngenetic or quasi-syngenetic period. According to the hydrocarbon potential analysis, the Late Ordovician Wufeng Formation and Lower Silurian Gaojiabian Formation are the source rocks in the high-maturity-over-maturity stage, the Carboniferous-Lower Permian carbonate is the good reservoirs, and the Late Permian Longtan-Dalong Formation is the stable seal, ensuring a huge hydrocarbon accumulation potential in SYSB. The methods proposed in this study can be applied to other carbonate-dominated strata worldwide.

1. Introduction

Carbonate strata contain approximately 70% of the global hydrocarbon reserves, 50% of the proven recoverable reserves, and 60% of the hydrocarbon production, making them essential for the hydrocarbon industry (Luo P et al., 2008; He ZL et al., 2011; Zhao WZ et al., 2014; Li Y et al., 2018). The exploration of hydrocarbons in marine carbonate rocks in China has a history of more than 40 years. Several large marine gas fields, including the Weiyuan (Wei GQ et

First author: *E-mail address*: hnwushuyu@163.com (Shu-yu Wu).
* Corresponding author: *E-mail address*: vnlj@163.com (Jun Liu).

Literary editor: Xi-jie Chen
doi:10.31035/cg2023059
2096-5192/© 2025 China Geology Editorial Office.

al., 2008; Zhou Q et al., 2014; Wang H et al., 2019), Puguang (Zhang XF, 2011; Lu P et al., 2022), Longgang (Qin SF et al., 2016; Huang CS et al., 2021), and Yuanba (Guo TL, 2018a; Guo XS et al., 2018b), have been discovered in the Sichuan Basin on the Upper Yangtze Platform (Ma YS et al., 2005, 2010; Zou CN et al., 2014; Zhao WZ et al., 2020; Yang Y et al., 2021). As an extension of the Lower Yangtze Platform in eastern China, the South Yellow Sea Basin (SYSB) is a multi-cycle superimposed basin on the Pre-Sinian metamorphic basement (Fig. 1a). The SYSB has a similar tectonic-paleogeography background and stratigraphic characteristics as the petroliferous Upper Yangtze region. However, it is the last large-scale sedimentary basin offshore China where no commercial hydrocarbon reservoirs have been discovered after long-time explorations (Zhao SJ et al., 2017; Lei BH et al., 2018; Xu M et al., 2019; Chen JW et al., 2020).

The boreholes and reflection seismic data confirmed that the Mesozoic-Paleozoic marine carbonate rocks were well developed in the Central Uplift of SYSB (Zhang YG et al., 2018; Cai LX et al., 2019, 2020). However, the Mesozoic-Paleozoic strata in the study area have experienced varying degrees of denudation and exfoliation due to intense Indosinian and Yanshan tectonic events (Shinn YJ et al., 2010; Tong J et al., 2018; Pang YM et al., 2021). In addition, carbonate reservoirs are highly heterogeneous during deposition and diagenesis (Bosence D, 2002; Behrooz ED and Hossain RB, 2009; Wennberg O et al., 2016; Masoud SY et al., 2019), resulting in complex carbonate reservoirs that are difficult to be statistically quantified. Therefore, the prediction of carbonate reservoirs is the key to hydrocarbon exploration in the SYSB, which needs to be further studied (Wu SY et al., 2016a, 2019; Nooshafarin H et al., 2020).

In predicting pore carbonate reservoirs, many studies performing petrophysical analysis argued that the matrix of carbonate rocks is heterogeneous and the pore structure is variable (Dai SH et al., 2006; Lei FL et al., 2010; Gao G, 2013a; Gao G et al., 2013b; Liu XX et al., 2013; Lei BH et al., 2018). The AVO forward modeling revealed that differences in porosity and oil-bearing properties in carbonate reservoirs could lead to significant AVO anomalies (Bao SH et al., 2003; Xie F et al., 2004; Ma LW et al., 2013). With the

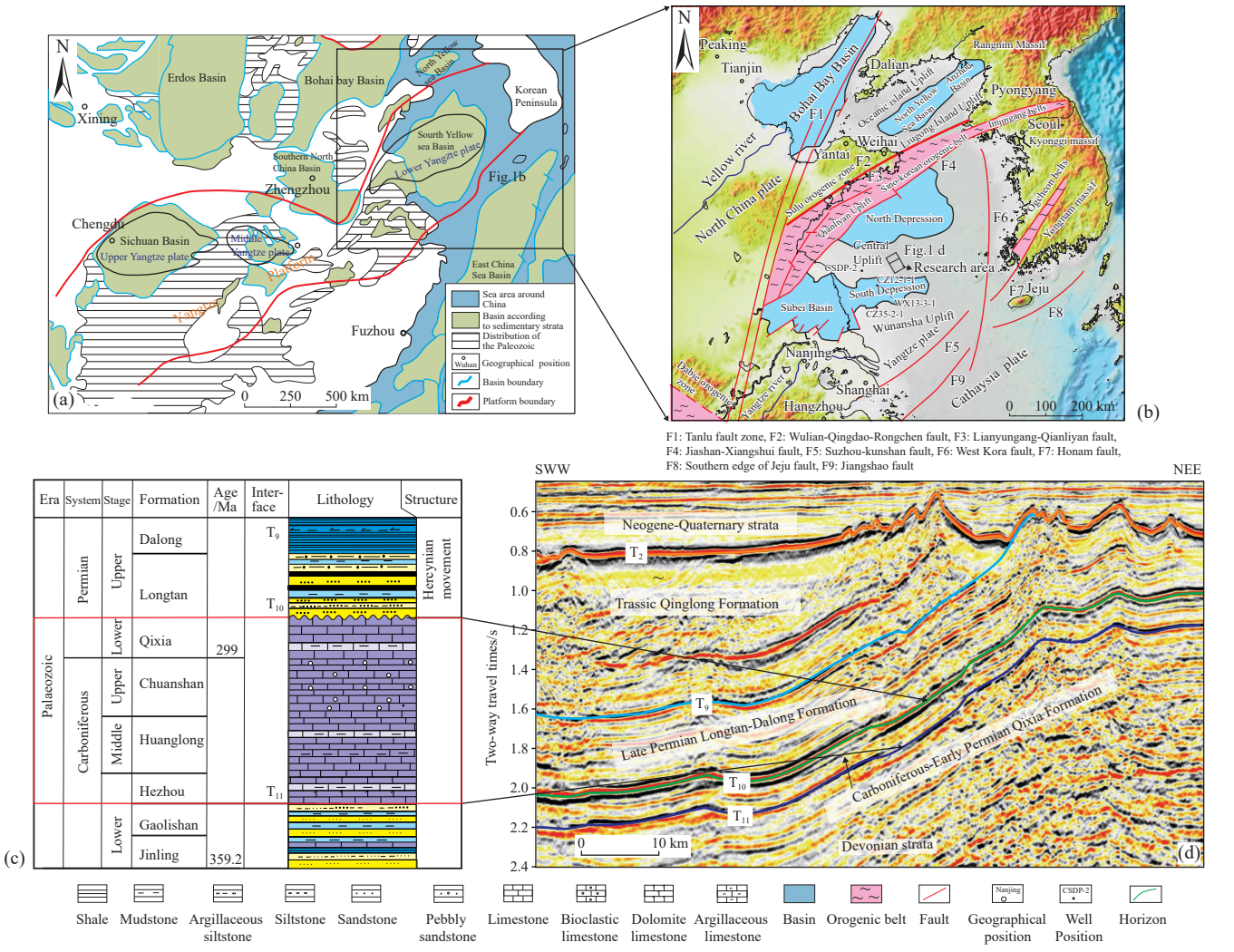

Fig. 1. Maps showing. a–Geographical location and tectonic map of the Yangtze block, South China (modified from Chen JW et al., 2020); b–geographical location and tectonic map of the SYSB (modified from Sheng QH et al., 2016); c–stratigraphic column shows the Carboniferous- Lower Permian; d–sedimentary facies of Upper Carboniferous Formation.

development of geophysical technology in recent years, technical methods, including seismic attributes analysis (Wang QC et al., 2008; Jiang XD et al., 2014; Liu GP et al., 2017; Zhao WZ et al., 2018), post-stack impedance inversion (Ma YS et al., 2005; Wang W et al., 2013; Du HK et al., 2017; Muhammad ZAD et al., 2021), pre-stack statistical inversion (Lv QB et al., 2012; Jin XJ et al., 2016; Zhang GR et al., 2017; Wang QT et al., 2019), pre-stack simultaneous inversion (Feng K et al., 2006), and phase-controlled constraints inversion (Ji XW et al., 2012; Chen ZQ et al., 2015; Li JL et al., 2017), have been effectively applied in the predication of carbonate reservoirs. In addition, the time-frequency analysis method has been gradually applied to carbonate reservoir prediction (Huang HX et al., 2003; Chen Y et al., 2013; Sheng QH et al., 2016), and the prediction of oil and gas bearing of the compound reservoir has been well verified (Yang ZC et al., 2017). The post-stack seismic attribute analysis and impedance inversion increase the multi-solution of reservoir prediction, making it more difficult to identify effective reservoirs. Post-stack seismic technology is generally based on the analysis of zero-offset channel stacking seismic data. To obtain the P-wave impedance, S-wave impedance, and density, pre-stack simultaneous inversion is performed using logging curves and pre-stack seismic data, which reflects amplitude change at various offsets or angles. Due to the heterogeneity of the carbonate reservoir in the study area, pre-stack inversion is the most effective technique to achieve accurate reservoir prediction.

To date, the prediction of carbonate reservoir in the SYSB, previous studies applied petrophysical analysis (Wu SY et al., 2016a, 2016b), seismic attribute analysis (Cao Q et al., 2008; Wu SY et al., 2011; Yuan Y et al., 2016), pre-stack inversion technique (Liu J et al., 2018; Wu SY et al., 2019) and time-frequency analysis (Wang JQ et al., 2016; Zhang XH et al., 2017). However, few studies have focused on the prediction of the pore carbonate reservoir in this area, especially in the Carboniferous- Lower Permian Formation. The mechanisms of the depositional environment also remain unclear. In this study, high-quality 3D seismic data and well data are used to explore the factors controlling the properties of Carboniferous-Early Permian carbonate reservoirs. The objectives of this study include: (1) Characterizing the porous carbonate reservoirs and predicting the distribution of favorable carbonate reservoirs; (2) analyzing the sedimentation through the δ^{18} O, δ^{13}C, and $^{87}Sr/^{86}Sr$ ratio; (3) modeling the distribution of porous carbonate reservoirs; (4) discussing the hydrocarbon potential of the Late Paleozoic assemblage. The results reveal the distribution and controlling factors of porous carbonate reservoirs, contributing to hydrocarbon exploration in the basin.

2. Geological setting

The SYSB is located in the continental margin of East Asia, and the basin is the offshore part of the Lower Yangtze Plate, bordered by the Qingling-Dabie-Sulu Orogenic Zone and the North China Plate to the north and the Jiangshao Orogenic Belt and Yangtze Plate to the south (Fig. 1a; Li WY et al., 2014; Shinn YJ, 2015; Wu SY et al., 2019). The SYSB region spans from 121°E to 124°E with an exploration area of about 180×10^3 km^2. Based on the size of the Mesozoic-Cenozoic sedimentary basin, the SYSB can be subdivided into five sub-tectonic units, including the Wunansha Uplift, the South Depression, the Central Uplift, the North Depression, and the Qianliyan Uplift from south to north, bounded by regional NE-strike and EW-strike faults (Fig. 1b; Liang J et al., 2017; Tong J et al., 2018; Pang YM et al., 2021; Cai LX et al., 2020; Duan SM et al., 2020). The SYSB stratigraphy consists of Archean-Proterozoic metamorphic rocks, Paleozoic to Triassic marine sediments, and Mesozoic-Cenozoic terrigenous sediments (Yao YJ et al., 2010; Liu J et al., 2018). The marine sedimentary sequences are spread across the entire basin, whereas the Mesozoic-Cenozoic continental sedimentary sequences are mainly developed in the South Depression and the North Depression areas (Pang YM et al., 2021).

The SYSB underwent six major stages of tectonic evolution: (1) Sinian-Early Ordovician plate expansion (passive continental margin basin) stage; (2) Late Ordovician-Silurian plate convergence, compression, and uplift (foreland basin) stage; (3) Late Devonian-Middle Triassic stable platform-intraplate rift stage; (4) Middle Triassic-Jurassic intracontinental uplift and compression (foreland basin) stage; (5) Cretaceous-Oligocene intracontinental extension-faulted stage; (6) Miocene to Quaternary intracontinental orogenic (depression basin) stage (Zhu WL et al., 2015; Lei BH et al., 2018). During the Mesozoic- Cenozoic, the tectonic framework of the East Asian continental margin was dominated by the West Pacific, Eurasian, and Indian plates (Zhang XH et al., 2019; Xu M et al., 2019).

Previous studies suggested that four regional source rocks were developed in the SYSB during the Mesozoic-Paleozoic period, including the Early Cambrian Hetang Formation, Late Ordovician Wufeng Formation, Early Silurian Gaojiabian Formation, and Late Permian Longtan-Dalong Formation (Zhu WL et al., 2020). The marine-facies reservoir was the main reservoir in the SYSB, including the Late Sinian Dengying Formation, Carboniferous-Late Permian Qixia Formation, and Early Triassic Qinglong Formation (Liang J et al., 2011; Wu SY et al., 2016a; Zhang YG et al., 2016). Three complete source-reservoir-caprock assemblages have been formed in the SYSB. Among the main assemblages, the Late Ordovician Wufeng Formation-Early Silurian Gaojiabian Formation is the source rock, the Middle-Late Silurian-Late Devonian Wutong Formation and Carboniferous-Early Permian Qixia Formation are the reservoirs, and the Late Permian Longtan-Dalong Formation is the caprock (Chen JW et al., 2019; Liang J, 2019). Only four wells (CZ35-2-1, CZ12-1-1, WX13-3-1, and CSDP-2) have been drilled through the Carboniferous-Early Permian strata (Chen JW et al., 2019; Guo XW et al., 2019; Zhang XH et al., 2019). Moreover, some hydrocarbons were identified in the core samples of the Carboniferous-Early Permian strata from the recent borehole CSDP-2, indicating the hydrocarbon potential of SYSB in the target layer (Feng ZQ et al., 2002; Hu F, 2010; Chen JW et al., 2018).

The Carboniferous-Early Permian strata include the

Carboniferous Hezhou Formation, Huanglong Formation, Chuanshan Formation, and Permian Qixia Formation. During this period, the SYSB was mainly marine deposition, with lithologies of limestone and dolomitic limestone (Fig. 1c). The Carboniferous-Early Permian strata are a set of reflection layers between T_{10} and T_{11} in the seismic profiles (Fig. 1d). T_{10} is the top surface with moderate-low frequency and high-amplitude positive reflections, and T_{11} is the bottom surface with moderate-low frequency and high-amplitude negative reflections. The internal seismic reflection of the Carboniferous-Early Permian strata is parallel-subparallel, characterized by continuous-moderate continuous frequency and moderate-amplitude seismic reflections. The overall strata thickness was relatively stable, ranging from 200 ms to 260 ms in time and 500 m to 715 m in depth. Due to the influence of the Late Indosinian tectonic movement, local highlands in the Carboniferous-Early Permian were denuded.

3. Data and methods

This study used high-quality 3D seismic data covering an area of 685 km^2, including 857 inlines and 2814 crosslines. The bin spacings were 25 m and 37.5 m in the inline and crossline directions, respectively. The seismic data was acquired using a 6390 cubic inch airgun in a water depth of 10 m and fired at 37.5 m intervals. The frequency range was 0 Hz to 80 Hz, the dominant frequency was about 35 Hz, and the P-velocity range was 5000 m/s to 6000 m/s. A high-resolution and high-fidelity seismic processing workflow (including statics correction, pre-stack noise suppression, deconvolution) was adopted to obtain the pre-stack time migration data.

Two wells (CSDP-2 and CZ12-1-1) were used in this study (Fig. 1b). The borehole CSDP-2 sampled 2843.18 m of continuous drilling through the Neogene, Triassic, Permian, Carboniferous, and Devonian strata. The borehole CZ12-1-1 was drilled to a total depth of 3511 m and penetrated through the Neogene, Permian, and Carboniferous strata (Fig. 1c). In order to extract sensitive parameters of the porous carbonate rock, a total of 15 core samples were collected from the Early Permian to Carboniferous strata (from a depth of 1647 m to 1960 m) of the borehole CSDP-2 for petrophysical parameter testing. The lithologies of all samples are mainly bioclastic limestone, pure limestone, sandstone, and mudstone, which were analyzed by the MTS815 spectrometer. It was equipped with high-precision pressure, displacement, volume change, temperature sensors, and ultrasonic transducers. P-wave velocity and S-wave velocity were tested under stratigraphic pressures, and the test conditions and data collection were controlled by a program of transmission method for measurement. According to the petrophysical equations, elastic parameters were calculated from P-wave velocity, S-wave velocity, and density. Subsequently, sensitive elastic parameters of physical properties were selected for further reservoir prediction.

Thirty-six (36) core samples of carbon and oxygen isotopes and 18 core samples of the strontium isotope from the borehole CSDP-2 were tested for sedimentary analysis. In order to avoid the diagenetic influences, samples from bioclastic, secondary fissures, calcite veins, recrystallization, and secondary transformation were excluded, and only pure limestones were tested. Carbon and oxygen isotopes were tested at the State Key Laboratory of Oil and Gas Reservoir Geology and Exploration (Chengdu University of Technology). A Thermo Fisher Stable Gas Isotope Mass Spectrometer MAT 253 was used with the phosphoric acid method. Afterward, strontium isotope analysis was conducted using a Triton Plus thermoelectric ionization isotope mass spectrometer.

3.1. Seismic inversion steps

According to the physical characteristics of carbonate rocks in the study area, an appropriate inversion method was selected to predict the distribution of the favorable reservoirs. The main factors affecting inversion results are geological conditions and methods, and the key factors of methods mainly include the quality of seismic data, wavelet extraction, low-frequency model establishment, and inversion parameters. Based on petrophysical analysis (lithological and property-sensitive elastic parameters), the pre-stack simultaneous inversion method was used to predict Carboniferous-Early Permian carbonate reservoirs. The steps of the pre-stack simultaneous inversion are as follows:

(i) The well-seismic data was calibrated according to near-middle-far angle superimposed gathers to obtain the near-middle-far seismic wavelets;

(ii) A low-frequency model was established to combine the velocity model from spatial interpolation of well points with the inversion results of high-precision tomographic velocity;

(iii) Based on the optimized near-middle-far gathers, the pre-stack simultaneous inversion method was employed to predict the lithology and physical properties of Carboniferous-Early Permian carbonate reservoirs;

(iv) Favorable distribution characteristics of porous carbonate reservoirs in the study area were obtained.

3.2. Calculation of paleosalinity and paleotemperature

Previous studies have shown that $\delta^{13}C$ and $\delta^{18}O$ generally increased with the paleosalinity (Clayton RN and Epstein S, 1958). Keith ML and Weber JN (1964) proposed a formula based on the relationship between the stable isotope $\delta^{13}C$ and $\delta^{18}O$:

$$Z = 2.048(\delta^{13}C + 50) + 0.498(\delta^{18}O + 50)(\text{PDB standard}) \quad (1)$$

where Z represents the paleosalinity, with Z >120‰ indicating the seawater-dominated sedimentary and Z <120‰ indicating the meteoric water-dominated sedimentary (Pekar SF et al., 2004; Sampei Y et al., 2005; Lécuyer C et al., 2012).

Paleotemperature is one of the important factors controlling the stable isotopic composition of carbonates. It can be effectively measured using $\delta^{18}O$ (Craig H, 1957):

$$T = 16.9 - 4.2(\delta^{18}O_{CaCO3\text{correct}} + 0.22 + 0.13\delta^{18}O_{CaCO3\text{correct}} + 0.22 \quad (2)$$

In the Paleozoic strata, a correction for the $\delta^{18}O$ "dating effect" is necessary. In general, the $\delta^{18}O$ value was calibrated from the average $\delta^{18}O$ of the Quaternary carbonate data (1.2‰). The average of $\delta^{18}O$ of the Early Permian-Carboniferous strata is −7.4‰, and the difference between them can be expressed as: $\Delta\delta^{18}O$ = 6.5‰, $\delta^{18}O_{CaCO3correct}$= measured value - $\Delta\delta^{18}O$. The paleotemperature of seawater can be calculated according to formula (2).

4. Results

4.1. Lithology and sedimentary environment

The lithology of the lower part of the Hezhou Formation is magenta bioclastic micritic limestone (Fig. 2a). The upper part is dominated by fine grey sandstone, and the topmost is medium-coarse lithic quartz sandstone with calcareous. Moreover, the medium-coarse quartz sandstone is supported by a grain structure with the main particle sizes ranging from 0.25 mm to 1 mm, with a high degree of roundness and good sorting. It contains crinoids, brachiopods, ostracoda, sea urchins, mollusks., etc., as well as more muddy cement. Therefore, the sedimentation was carried out from deep water to relatively shallow water, and the depositional environment was tidal flat with an open carbonate platform, consistent with the Chaohu area in Anhui Province (Li SY et al., 2015).

The lithology of the Huanglong Formation is dominated by gray-brown and light grey bioclastic micritic limestone (Fig. 2a). The bioclastic limestone consists of fusulinida, cephalopods, and brachiopods, with a light flesh-red limestone at the bottom and minor gravel limestone and oolitic limestone. The lithology of the lower part is composed of micritic calcite (Fig. 2a), with numerous silty clastic particles in the micritic calcite crystal aggregates. The sediments are confined to the platform lagoon environment. The lithology of the upper part is spheroidal with bio-fossils. The spherulitic micritic limestone is filled with sparry calcite crystals, and the depositional environment is a shallow open platform beach with high energy turbulence.

The lithology of the Chuanshan Formation is a black-grey and dark-grey bioclastic micritic limestone with abundant nucleate stones (Fig. 2a). The limestone consists of many bio-fossil fragments filled with micro calcite crystals, with well-developed microfractures between bio-fossil fragments. The lithology is almost micrite or micrystallinne with pane fabric or bird's eye structures, and the depositional environment is an open platform tidal flat.

The lower part of the Qixia Formation consists of fine-grained clastic rocks, characterized by black mudstone intermixed with grey calcareous silt-fine sandstone and thin black coal seams (Fig. 2a). The middle part consists of swinestone (a black bituminous argillaceous limestone), and the upper part is dark-grey limestone (Fig. 2a). This formation developed fossil spindles, fossil corals, foraminifera, and a considerable amount of biological debris, indicating relatively stable water energy and normal salinity for biological growth. The depositional environment was a shallow-water carbonate platform.

4.2. Types of reservoir space

The Lower Permian-Carboniferous Formation is dominated by micritic limestone, with the reservoir space consisting of intergranular pores, dissolution pores, karst caves, sutures, and fractures.

Intergranular pores mainly exist in carbonate grains. According to grain types, the pores can be categorized into inter-oolitic pores, sand pores, and inter-clastic pores. After diagenesis, most of the pores are filled with biodetritus (Figs. 2b and k) and sparite calcite (Fig. 2l) due to cementation. Under single polarized light, the grain appears dark orange light, with only a few residual intergranular pores (Figs. 2b, k, l).

The bioclastic limestone and micrite limestone contained dissolution pores, which were formed by atmospheric water leaching based on primary pores. The pores were connected by dissolution fractures, ranging in size from 40 μm to 100 μm, and most of the dissolution pores were unfilled (Figs. 2e and s).

The study area is rich in karst caves with various morphologies and shapes. Most caves are isolated, some are filled with calcite or bioclastic limestone (Figs. 2d and h), and others are unfilled (Figs. 2c, n, p).

Suture lines form predominantly in the micritic limestones with abundant bioclasts. Most suture lines are residual gaps formed by pressure dissolution (Figs. 2r and u), and some of them are filled with mud. The gaps can be used as hydrocarbon migration channels.

Fractures developed in the intergranular, suture lines, and fissures are fully filled (Figs. 2g, h, j, o) or semi-filled (Fig. 2q) with micritic calcite, while some fractures are not filled (Figs. 2f, l, m, n, t). Unfilled fractures can connect pores and increase the permeability of the rocks.

4.3. Reservoir physical property

The borehole CZ12-1-1 is used for the log-seismic characteristic analysis (Fig. 3). The Chuanshan Formation was drilled to a depth of 2069 m to 2212 m, with a thickness of 137 m, mainly composed of bioclastic limestone. The P-wave velocity in this formation ranges from 5000 m/s to 6000 m/s, and the density ranges from 2.3 g/cm^3 to 2.6 g/cm^3. The P-wave impedance is between 16000 g/cm^3·m/s and 17000 g/cm^3·m/s. The Sanduo Formation above the Chuanshan Formation comprises clastic rocks with a P-velocity of 3000 m/s–4000 m/s and a density of 2.2 g/cm^3–2.4 g/cm^3. Its P-wave impedance ranges from 7000 g/cm^3·m/s to 8000 g/cm^3·m/s. The P-wave velocity, P-wave impedance, and density of the clastic rocks in the Sanduo Formation are much lower than those of the bioclastic limestone in the Chuanshan Formation. The limestone is characterized by low-medium frequency, weak amplitude, and semi-continuous/continuous seismic reflections.

The P-wave velocity, S-wave velocity, and saturated water density were obtained through the petrophysical parameter

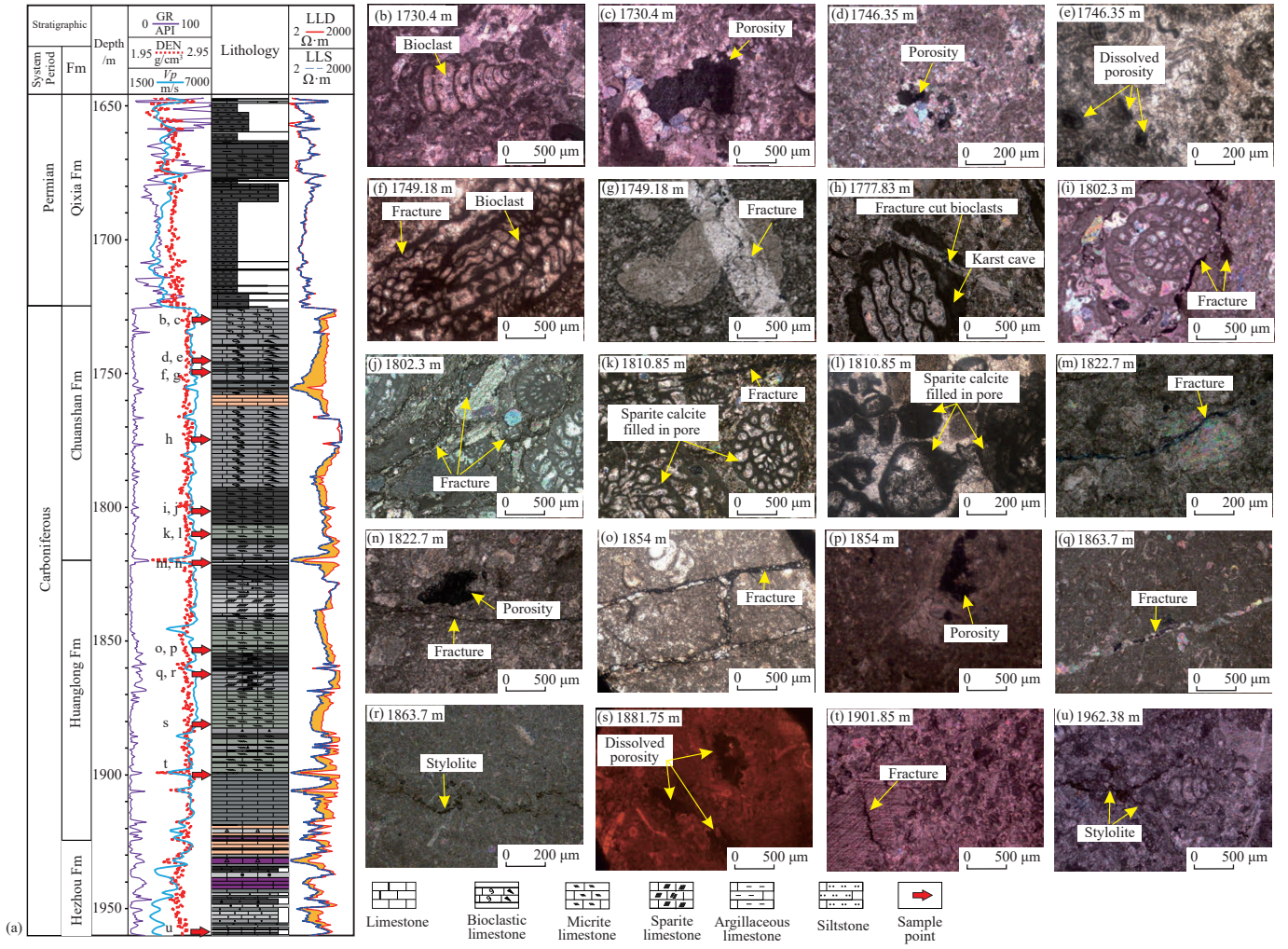

Fig. 2. Lithologic column and different types of pores in the Lower Permian-Carboniferous strata. a–Lithologic column and logging curve of the borehole CSDP-2. Arrows indicate the sample points. b–bioclastic micritic limestone, shuttle alga fossil at 1730.4 m of Chuanshan Formation (single polarized light); c–bioclastic micritic limestone, sparry calcite partially filled in the karst cave at 1730.4 m of Chuanshan Formation (single polarized light); d–micrite limestone, sparry calcite partially filled in the karst cave at 1746.35 m of Chuanshan Formation (single polarized light); e–bioclastic limestone, intergranular dissolution pores at 1746.35 m of Chuanshan Formation (single polarized light); f–bioclastic micritic limestone, clay rocks filled in the fracture, clostridium fossils at 1749.18 m of Chuanshan Formation (single polarized light); g–bioclastic micritic limestone, structural fracture developed, sparry calcite in raw debris at 1749.18 m of Chuanshan Formation (single polarized light); h–bioclastic micritic limestone, sparry calcite in bioclasts, the large grain size of raw debris, karst cave developed and partially filled with sparry calcite at 1777.83 m of Chuanshan Formation (single polarized light); i–bioclastic micritic limestone, fracture developed at 1802.3 m of Chuanshan Formation (single polarized light); j–bioclastic micritic limestone, fractures filled with calcite, visible argillaceous bands at 1802.3 m of Chuanshan Formation (single polarized light); k–bioclastic micritic limestone, fracture developed, bioclastic coelom pores filled with sparry calcite at 1810.85 m of Chuanshan Formation (single polarized light); l–oolitic limestone, sparite calcite filled in the pores with dark orange light at 1810.85 m of Chuanshan Formation (single polarized light); m–endoclastic micritic limestone, fracture developed at 1822.7 m of Huanglong Formation (single polarized light); n–endoclastic micritic limestone, fracture partially filled with argillaceous material, micritic calcite as main interstitial material, dissolution pores developed at 1822.7 m of Huanglong Formation (single polarized light); o–micrite limestone, multiple fractures developed, filled with calcite and mud at 1854 m of Huanglong Formation, (single polarized light); p–micrite limestone, developed crinoids and foraminifera fossil and dissolved pore at 1854 m of Huanglong Formation (orthographic photograph); q–bioclastic micritic limestone, fracture developed and filled with sparry calcite at 1863.7 m of Huanglong Formation (single polarized light); r–bioclastic micritic limestone, suture lines developed, partially filled with mud at 1863.7 m of Huanglong Formation (single polarized light); s–micrite limestone, dissolution pores developed, cathode luminescence at 1881.75 m of Huanglong Formation; t–bioclastic sparry limestone, bioclastic rich and fracture developed, fracture partially filled with sparry calcite and mud at 1901.85 m of Huanglong Formation (single polarized light); u–bioclastic micritic limestone, suture lines developed, biodetritus and sutures cut by late structural fractures at 1962.38 m of Hezhou Formation (single polarized light).

tests (Table. 1; Fig. 4). The P-wave velocity ranges from 5075 m/s to 6568 m/s, S-wave velocity ranges from 2551 m/s to 3432 m/s, and saturated water density ranges from 2.582 g/cm^3 to 2.761 g/cm^3. The comparison of the P-velocity of well logging (green dotted line) with that from the petrophysical parameter test (black red bar) shows a good fit (Fig. 4a), indicating that the test results are accurate.

Based on the core test data of the borehole CSDP-2 (Table. 1) and the intersection of P-wave impedance and S-wave impedance (Fig. 4b), the authors observed that the P-

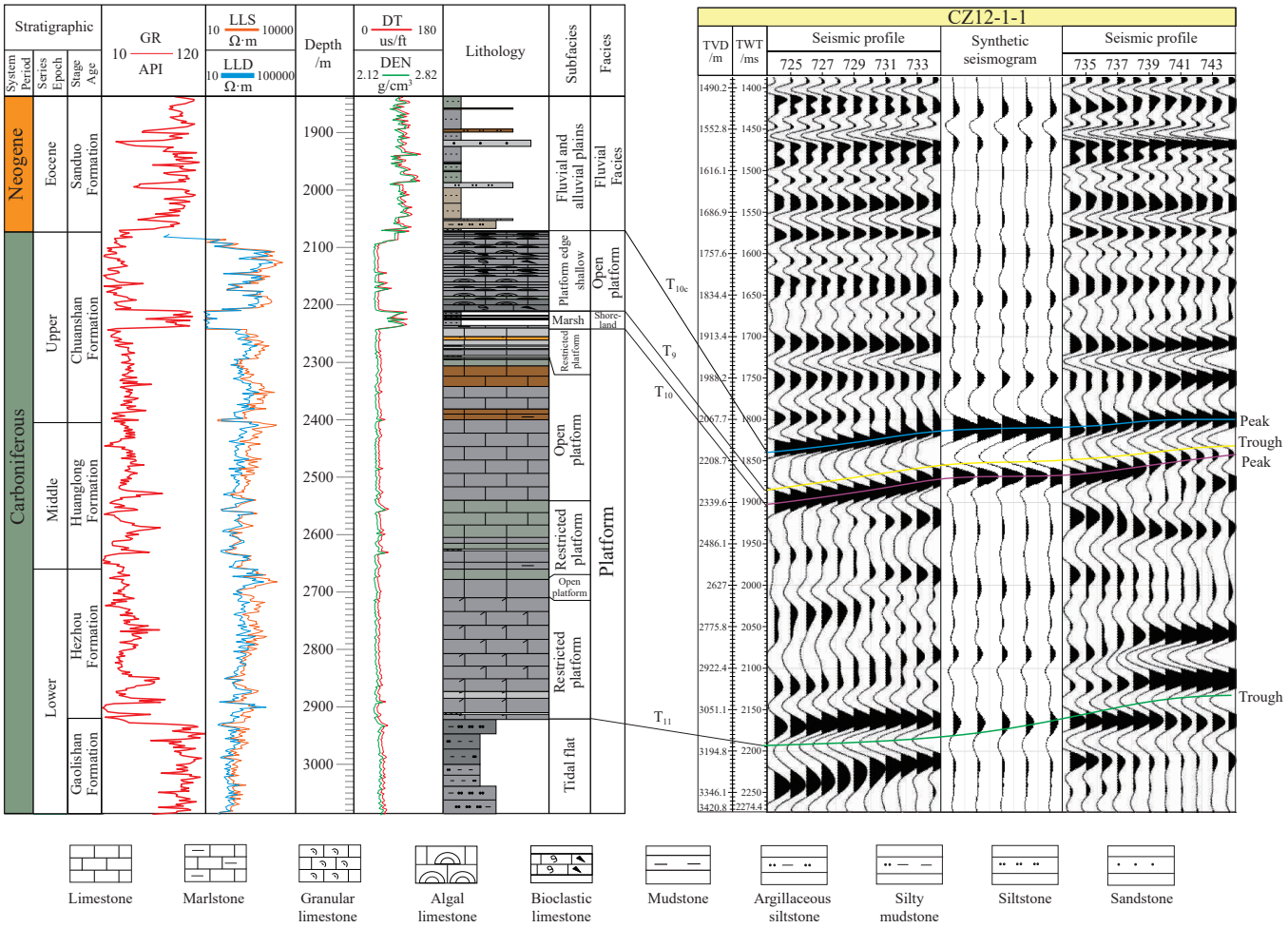

Fig. 3. Log characteristic and seismic reflection of bioclastic limestone in well CZ12-1-1.

Table 1. P-wave velocity, S-wave velocity, and density of borehole CSDP-2 based on petrophysical parameter testing.

Stratum	Depth /m	Lithology	Formation pressure /MPa	P-wave velocity /(m/s)	S-wave velocity /(m/s)	Saturated water density /(g/cm^3)
Qixia Fm	1647.5	Argillaceous limestone	37	6568.8	3372.1	2.761
Qixia Fm	1667.5	Micrite limestone	37	5864	3257.8	2.677
Qixia Fm	1684.1	Mudstone	38	5075.1	2551.7	2.624
Qixia Fm	1713.4	Mudstone	38	6270.5	3217.8	2.756
Chuanshan Fm	1733.3	Bioclastic limestone	39	6171	3028.5	2.597
Chuanshan Fm	1767.4	Bioclastic limestone	39	6303.1	3368.5	2.656
Chuanshan Fm	1801.68	Crystallite limestone	40	5931	2947.9	2.596
Chuanshan Fm	1816.5	Crystallite limestone	41	6261.3	3000.6	2.671
Huanglong Fm	1830.18	Micrite limestone	41	6511.4	3160.3	2.617
Huanglong Fm	1844.9	Micrite limestone	41	5939.2	3431.1	2.603
Huanglong Fm	1867.1	Micrite limestone	42	6100	3223.4	2.711
Huanglong Fm	1908.3	Limestone	43	6201.3	3411.8	2.644
Hezhou Fm	1935.8	Limestone	43	5701.7	3341.7	2.618
Hezhou Fm	1939.85	Clot limestone	43	5628.1	2802.5	2.644
Hezhou Fm	1958.08	Greyish fine sandstone	44	5183.6	2877.9	2.582

Note: Fm: Formation

wave impedance can distinguish the lithology of bioclastic limestone, pure limestone, and clastic rock. The P-wave impedance of clastic rock value ranges from 10000 g/cm^3·m/s to 14500 g/cm^3·m/s, while the impedance values of pure limestone are much higher than those of clastic rocks, ranging from 13800 g/cm^3·m/s to 16300 g/cm^3·m/s. The maximum values of bioclastic limestone range from 16300 g/cm^3·m/s to 17500 g/cm^3·m/s. Based on the above results, P-wave impedance is a sensitive lithology parameter.

The intersection analysis shows that as the porosity

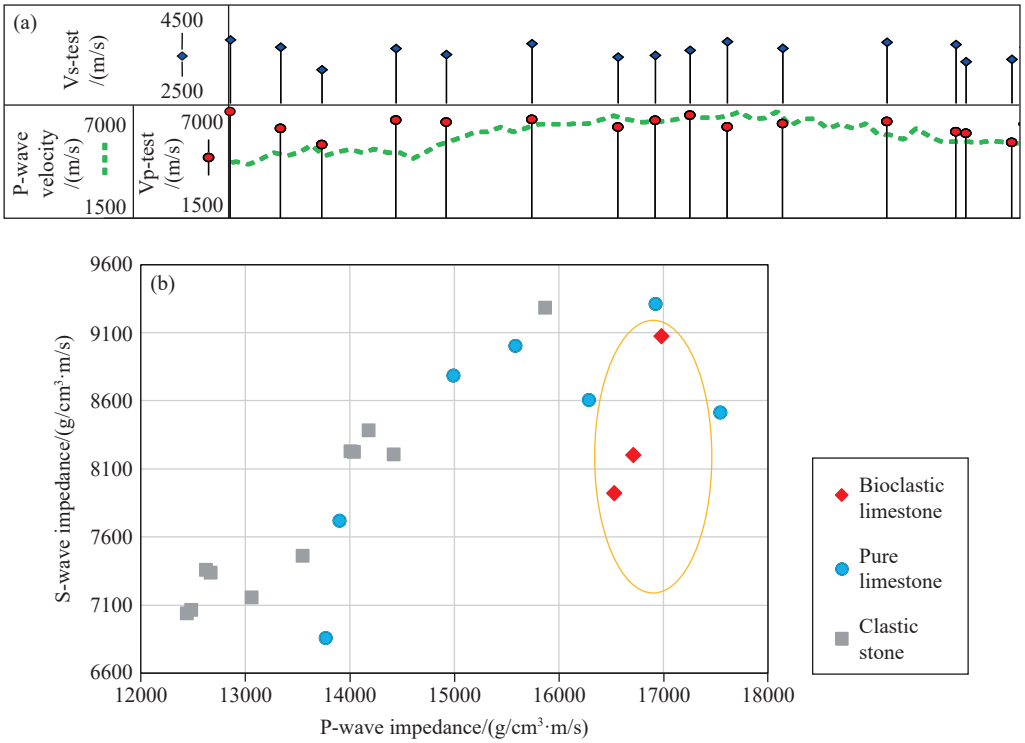

Fig. 4. a–P-wave velocities from CSDP-2 well logs and petrophysical parameter test, and S-wave velocities from petrophysical parameter tests; b–Analysis of lithology sensitive parameters in the borehole CSDP-2.

increases, the Lamet constant (λ), Poisson ratio (v) (Fig. 5a), P-wave impedance, bulk modulus (K) (Fig. 5b), shear modulus (μ), and P-wave velocity (Fig. 5c) decrease. However, relying solely on these elastic parameters for property differentiation may lead to a certain degree of overlap. The limestone with low Lamet constant ×density ($\lambda\rho$) and shear modulus×density ($\mu\rho$) has good physical properties (Fig. 5d). Since $\lambda\rho$ allows a clear distinction between good and poor reservoirs, it was selected to determine the physical properties of the reservoirs through its intersection with the porosity of limestone in the targeted formation (Fig. 5e). The obtained linear relationship is $\varphi = \lambda\rho \times 10^{-9} + 1.3052$.

Based on the core samples from the borehole CSDP-2, the porosities of the Carboniferous Formation range from 0.89% to 4.36%, with an average porosity of 2.05%. In addition, the permeability ranges from 0.15×10^{-3} mD to 3.80×10^{-3} mD, with an average permeability of 1.38×10^{-3} mD (Table. 2). These petrophysical test results indicate a low porosity and permeability of the Carboniferous Formation reservoirs. Bioclastic micritic limestone in the Chuanshan Formation and Huanglong Formation has a high porosity (1.51%–4.36%), while the porosity (0.89%) of the Hezhou Formation is low (Table. 2).

4.4. Porous carbonate distribution

The ultimate goal of seismic inversion is to predict the distribution and physical properties of carbonate reservoirs quantitatively and semi-quantitatively. Based on the pre-stack seismic data at different angle gathers, low-frequency models of P-wave impedance, S-wave impedance, and density are used to constrain and implement the pre-stack simultaneous inversion. The elastic parameter data for the lithologic and physical properties are obtained (Figs. 6a and b).

According to the results of petrophysical analysis, the threshold of P-wave impedance (13500 g/cm^3·m/s) is used to distinguish clastic rocks from limestone, and the threshold of P-wave impedance (16300 g/cm^3·m/s) is used to distinguish bioclastic limestone from pure limestone. The results show that the bioclastic limestone reservoirs of the Carboniferous-Early Permian Formation are well developed, mainly in the Hezhou Formation and the Chuanshan Formation, partly in the Qixia Formation (Fig. 6a).

As shown in Fig. 5d, the physical properties $\lambda\rho$ between 30×10^6 (kg^2/m^2·s) to 70×10^6 (kg^2/m^2·s) represent the favorable reservoirs in the limestone. Red and yellow represent optimal physical properties, and green and blue indicate poor physical properties (Fig. 6). According to the P-wave impedance threshold, the impedance ranges of clastic rock and pure limestone are excluded, and the relationship between $\lambda\rho$ and porosity is obtained from petrophysical analysis (Fig. 5e). Finally, the porosity data of bioclastic limestone reservoirs are obtained (Fig. 6c). The Carboniferous-Early Permian porous carbonate reservoirs exhibit strong spatial heterogeneity. For vertical distribution, good reservoirs are mainly developed on the slope of the Hezhou Formation, the paleo-highland of the Huanglong Formation, and the Chuanshan Formation (Fig. 6d). In lateral distribution, the carbonate reservoirs with good physical properties are located around the NE-oriented paleo-highland (Fig. 6c), with porosity ranging from 3% to 5%.

According to borehole CSDP-2, oil traces were observed

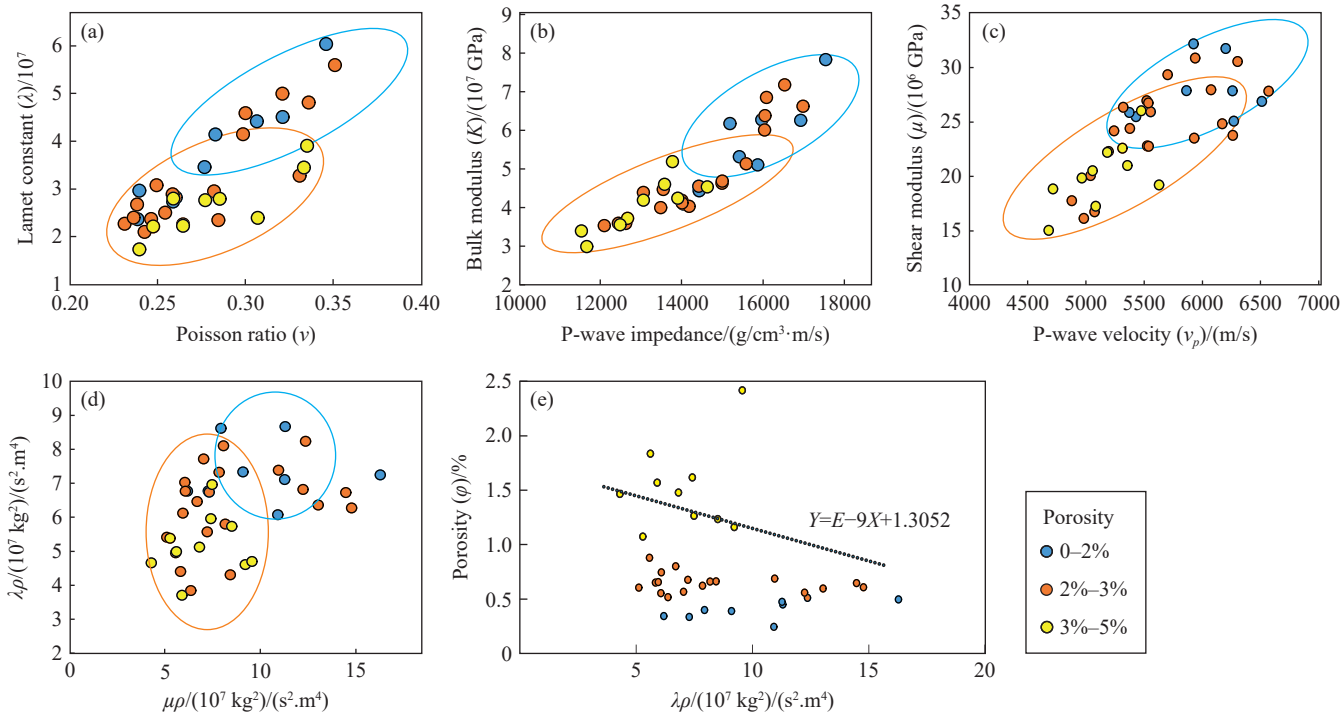

Fig. 5. Property sensitive parameters from borehole CSDP-2. a–Intersection of Lamet constant and passion ratio; b– intersection of P-wave impedance and bulk modulus; c–intersection of P-wave velocity and shear modulus; d–intersection of shear modulus×density ($\mu\rho$) and lamet×density ($\lambda\rho$); e–intersection of lamet×density ($\lambda\rho$) and porosity of bioclastic limestone of the Carboniferous-Early Permian Formation.

Table 2. Petrophysical properties of the Carboniferous Formation.

Stratum	Depth/m	Lithology	Porosity/%	Permeability /mD
Chuanshan Fm	1802.48	Sparite bioclastic limestone	1.51	0.69×10^{-3}
Chuanshan Fm	1807.38	Sparite bioclastic limestone	1.53	0.78×10^{-3}
Chuanshan Fm	1809.65	Bioclastic micritic limestone	2.87	0.65×10^{-3}
Chuanshan Fm	1812.48	Bioclastic microcrystalline limestone	4.36	1.40×10^{-3}
Huanglong Fm	1868.62	Argillaceous microcrystalline limestone	1.49	1.20×10^{-3}
Huanglong Fm	1892.90	Microcrystalline limestone	1.81	3.80×10^{-3}
Huanglong Fm	1894.08	Bioclastic micritic limestone	1.70	0.15×10^{-3}
Huanglong Fm	1899.60	Bioclastic micritic limestone	2.99	1.25×10^{-3}
Huanglong Fm	1904.88	Micritic microcrystalline limestone	1.33	1.16×10^{-3}
Hezhou Fm	1962.38	Bioclastic micritic limestone	0.89	/

in the fissures, the middle of grey-brown bioclastic limestone (Fig. 6e), and the bottom of dark grey bioclastic limestone (Fig. 6f). Oil immersion was also detected in the grey-black bioclastic limestone with siliceous bands at the top of the Huanglong Formation and in the algal limestone at the middle (Fig. 6g). Furthermore, oil traces were found in the grey-black micritic limestone at the top of the Hezhou Formation, with the emergence of numerous fractures (Fig. 6h). The drilling results are consistent with the reservoir predictions.

4.5. Isotope results

The preservation status of bulk carbonate samples was verified by the correlation between $\delta^{18}O$ and $\delta^{13}C$. Since R>0.5 suggests diagenetic changes, bulk samples with R>0.5 were altered. The bulk carbonate samples from all investigated sections indicate no significant correlation between $\delta^{18}O$ and $\delta^{13}C$ (R = 0.24; Fig. 7). Furthermore, the $\delta^{18}O$ value significantly decreased after diagenesis in response to atmospheric fresh water and hydrothermal fluids. When $\delta^{18}O$ <−5‰, the carbonate rocks underwent diagenetic alteration, but their carbon and oxygen isotopic compositions still represented the seawater at that period. When $\delta^{18}O$<−10‰, the rocks underwent a strong diagenetic transformation without sample values of carbon and oxygen isotopes. From the Early Permian to Carboniferous Formation, $\delta^{18}O$ ranges between −10.55‰ and −5.65‰, with a mean value of −7.4‰. Except for two samples with $\delta^{18}O$ <−10‰ (at a depth of 1723.73 m and 1948.5 m), all other samples have $\delta^{18}O$ values between −9.75‰ and −5.65‰ (Fig. 7). This result indicates that though the oxygen isotopes can still represent the original sedimentary despite the influence of diagenesis.

In the Carboniferous-Early Permian Formation, the

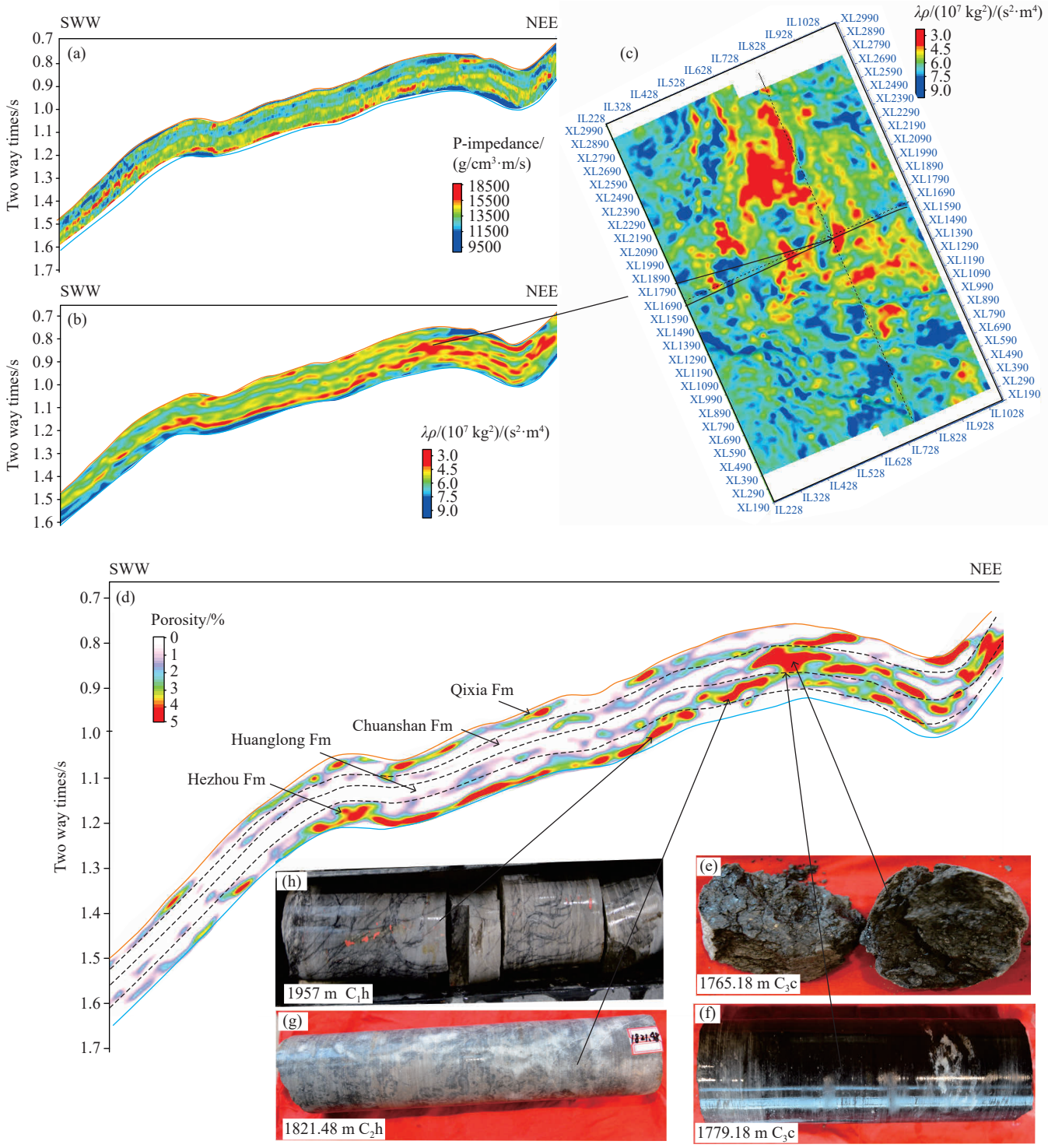

Fig. 6. Carboniferous-Early Permian porous carbonate reservoirs prediction. a–P-wave impedance profile showing the lithologic distribution; b–λρ profile showing the physical properties; c–physical characteristics of Carboniferous-Lower Chuanshan Formation; d–porosity profile; e–oil traces in the grey-brown bioclastic limestone at a depth of 1765.18 m of borehole CSDP-2; f–oil trace in the dark grey bioclastic limestone at a depth of 1779.18 m of borehole CSDP-2; g–oil immersion in the grey-black bioclastic limestone; h–oil traces in the grey-black micritic limestone at a depth of 1821.48 m of borehole CSDP-2.

paleosalinity is between 110‰ and 132‰, with a mean value of 124‰; the paleotemperatures vary between 13.74°C and 36.46°C, with a mean value of 21.44°C (Fig. 8); the $\delta^{13}C$ is between −6.24‰ and 4.39‰, with a mean value of 0.158‰ (Fig. 9). The ratio of $^{87}Sr/^{86}Sr$ is between 0.71 and 0.73, with a mean value of 0.71 (Fig. 8). Overall, the $^{87}Sr/^{86}Sr$ ratio of test samples is significantly higher than that derived from the mantle, which has a mean value of 0.70. The high $^{87}Sr/^{86}Sr$ ratio may indicate the influence of terrigenous diagenetic fluids and clastic types of cement with a higher $^{87}Sr/^{86}Sr$ ratio on carbonate (Armstrong-Altrin JS et al., 2009).

The paleotemperature of the Hezhou Formation increased

from 24.6°C to 36.46°C and then decreased from 36.46°C to 25.49°C with paleosanity <120‰, which is continuously affected by terrigenous sources. $\delta^{18}O$ is between −10.55‰ and −8.16‰, with two negative $\delta^{13}C$ excursion values exhibited accompanied by the last sea level falling (Fig. 8).

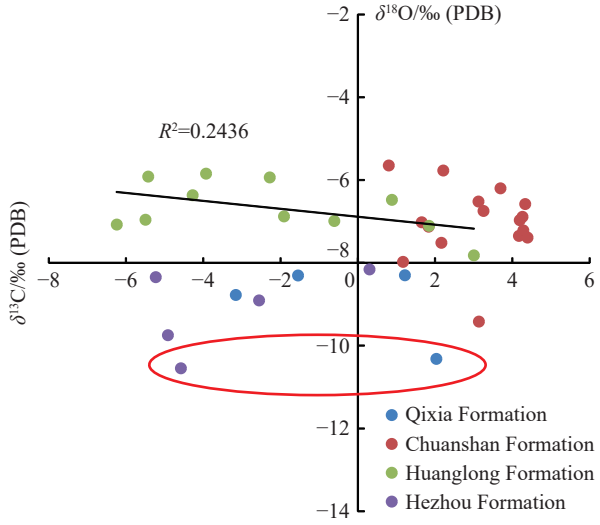

Fig. 7. Intersection of $\delta^{18}O$ and $\delta^{13}C$ in the Carboniferous-Early Permian Formation from borehole CSDP-2.

The paleotemperature of the Huanglong Formation was relatively stable, ranging from 14.55°C to 23.03°C, with paleosanity fluctuating around 120‰ (a value ranging from 110.9‰ to 129.5‰), corresponding to sea-level fluctuations (Li SY et al., 2015). The $\delta^{18}O$ is between −7.82‰ and −5.94‰, with two negative $\delta^{13}C$ excursion values, and the last sea-level regression exhibits a high $^{87}Sr/^{86}Sr$ ratio (Fig. 8).

The paleosanity during the whole Chuanshan period is greater than 120‰, indicating the existence of marine sediments (Fig. 8). During the Early-Middle Chuanshan period, paleotemperature is between 15.98°C and 23.77°C, $\delta^{18}O$ ranges from −5.65‰ to −7.98‰, and $\delta^{13}C$ is relatively stable (Fig. 8). At the end of the Chuanshan period, the paleotemperature reaches two peaks (30.67°C and 35.26°C), along with the highest sea level. $\delta^{18}O$ experiences an abnormally negative shift, accompanied by a high $^{87}Sr/^{86}Sr$ ratio.

The paleotemperature of the Qixia period is between 25.3°C and 27.54°C, and the paleosanity fluctuates around 120‰ (between 116.46‰ and 125.67‰). $\delta^{18}O$ ranges from −8.3‰ to −8.78‰ (Fig. 8). At the beginning of this period, the $\delta^{18}O$ value gradually increases, and the paleosalinity and paleotemperature decreases, accompanied by the falling of the sea level (Ross CA and Ross JRP, 1987, 1995). During the

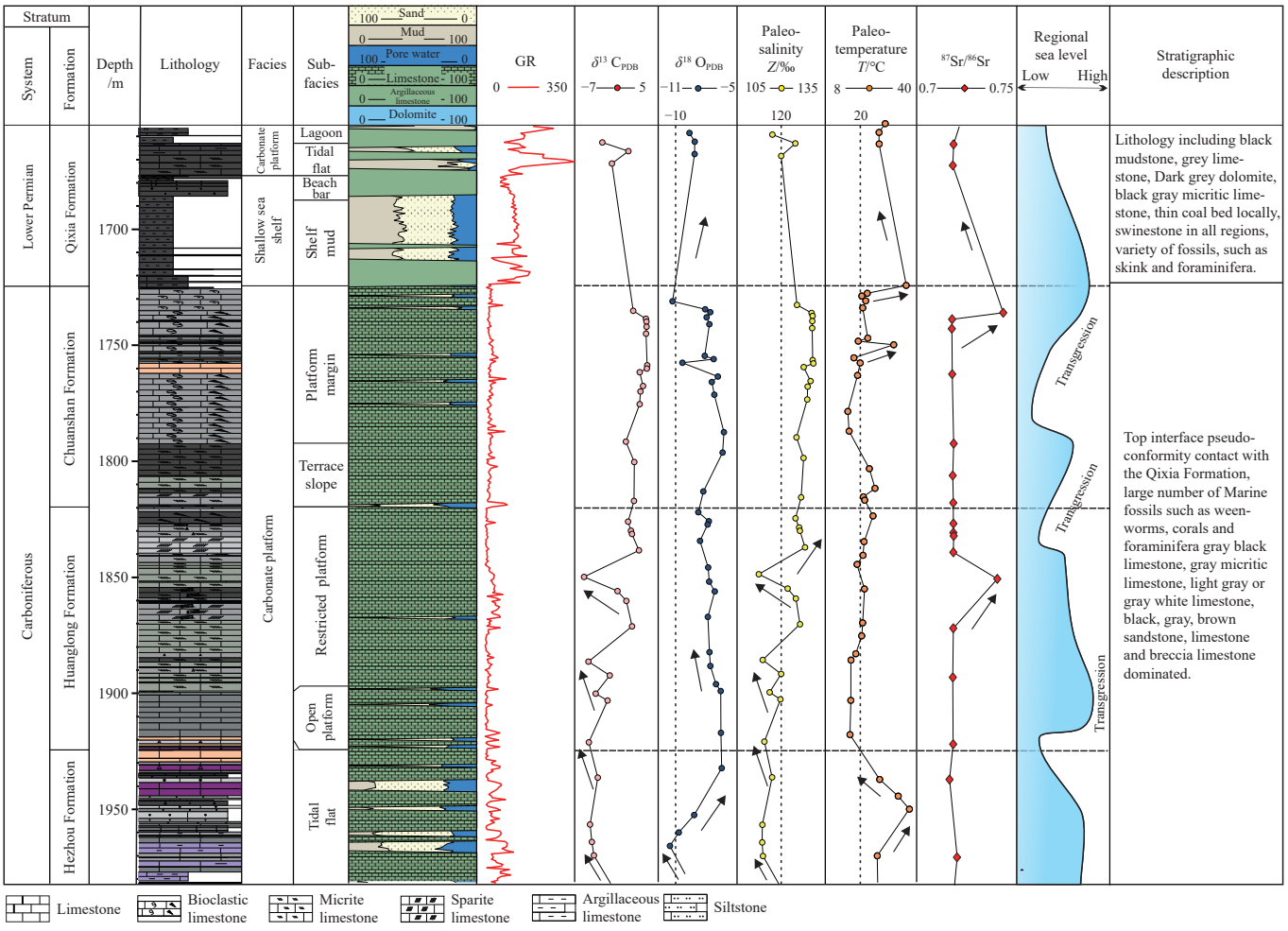

Fig. 8. Carbon, oxygen, and strontium isotope compositions of the Carboniferous-Early Permian Formation.

late period, the $\delta^{18}O$ value decreases and the paleosalinity and paleotemperature increases (Fig. 8).

5. Discussion

5.1. Sedimentation analysis and porosity discussion

The Yangtze Plate is located near the equator in the southern hemisphere, at the eastern edge of the Carboniferous-Early Permian Paleotethys Ocean, with a latitude ranging from 1.6°S to 2.4°N (Mcelhinny MW, 1985; Shi GR and Chen ZQ, 2006; Zhao MY and Zheng YF, 2014; Wu YW et al., 2021).

In the Carboniferous period, the southwest and the southeast of the Yangtze Plate were significantly influenced by the Paleotethys tectonic domain. During the Carboniferous period, there were three regional sea-level fluctuations on the Yangtze Plate, which was a cycle of gradual uplift (Fig. 8; Wang XD et al., 2019). In the Early Carboniferous global transect period, the Lower Yangtze Plate and Cathaysia Plate were connected into a large carbonate platform until the end of the Chuanshan period. The SYSB began to subside in the early period of the Carboniferous (Chen HC et al., 1979; Wang CS et al., 1999). The warm and humid tropical climate with abundant atmospheric precipitation facilitated carbonate deposition (Feng ZZ et al., 1993; Li SY and Jin FQ, 1994; Shi et al., 2006). Previous studies of Carboniferous-Early Permian sedimentary sequences at low latitudes in South China (Li RF et al., 1997; Qie WK et al., 2011; Wu SY et al., 2016a), North America (Heckel PH, 1986; Smith JLB and Read JF, 2000; Feldman HR et al., 2005) and Euramerica (Veevers JJ and Powell CM, 1987) have shown that the sequence architecture and implied eustatic fluctuations of the lower latitude regions (e.g. South China and Southwestern USA) correspond well to the Late Palaeozoic Gondwanan glaciation.

The Central Uplift of SYSB was considered a paleo-uplift after the Caledonian period, and the borehole CSDP-2 identified shoal-reef facies developed in local highlands (Chen JW et al., 2016; Gao XH et al., 2020). However, the sea level of the lower Yangtze Plate was deeper than the upper Yangtze Plate during the Carboniferous period (Chen JW et al., 2016). Therefore, shoal reef facies of porous reservoirs were mainly developed at the edge of the SYSB platform uplift, enclosed by an open shelf.

Seawater intruded from east and west of the SYSB during the late Early Carboniferous (from 323.2±0.4 Ma to 330.9±0.Ma; Sheng QY et al., 2013; Hong HL et al., 2014), with a typical hot and humid weather (temperatures between 24.6°C and 36.46°C). During the Hezhou period, the SYSB was in a shallow shelf and tidal-flat environment with an NNE trend, forming delta facies near the shore (Fig. 10a). Two small amplitude negative $\delta^{13}C$ excursions indicate two brief glaciations, resulting in lower sea level and lower salinity (Fig. 8). With a decreasing sea level, sedimentary paleo-uplift were susceptible to superimposed syngenetic and quasi-syngenetic exposures (Fig. 6h; Zhao MY and Zheng YF, 2014). It was subjected to diagenetic alteration and affected by leaching and dissolution of the freshwater, leading to the increase of pore space (Fig. 2u; Wang CS et al., 1999). Considering more accumulation space in the southwestern slope zone, the shoals began to superimpose and continued to migrate seaward, with good development and distribution of shoal reservoirs in the slope zone (Fig. 6d).

A big transgression occurred in South China during the Late Carboniferous (from 307±0.1 Ma to 323.2±0.4Ma), and the Yangtze Sea and the Paleo-South China Sea were almost connected (Li SY et al., 2015; Li N et al., 2021) with a warm weather (14.55°C to 23.03°C). The SYSB was in a platform margin, restricted platform, and tidal-flat environment (Fig. 10b). The lithology of Huanglong Formation is mainly pure

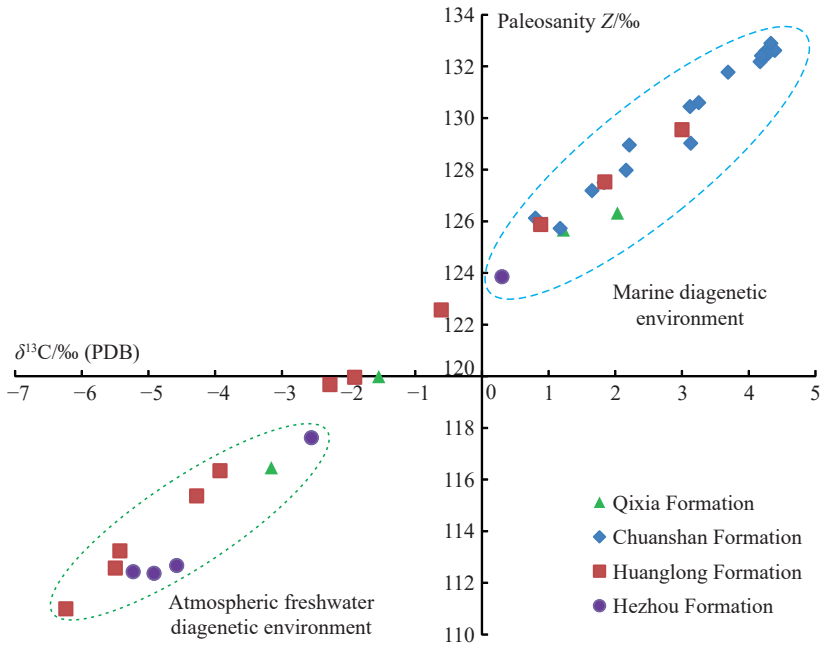

Fig. 9. Intersection of carbonate *versus* paleosalinity of the Carboniferous-Early Permian Formation.

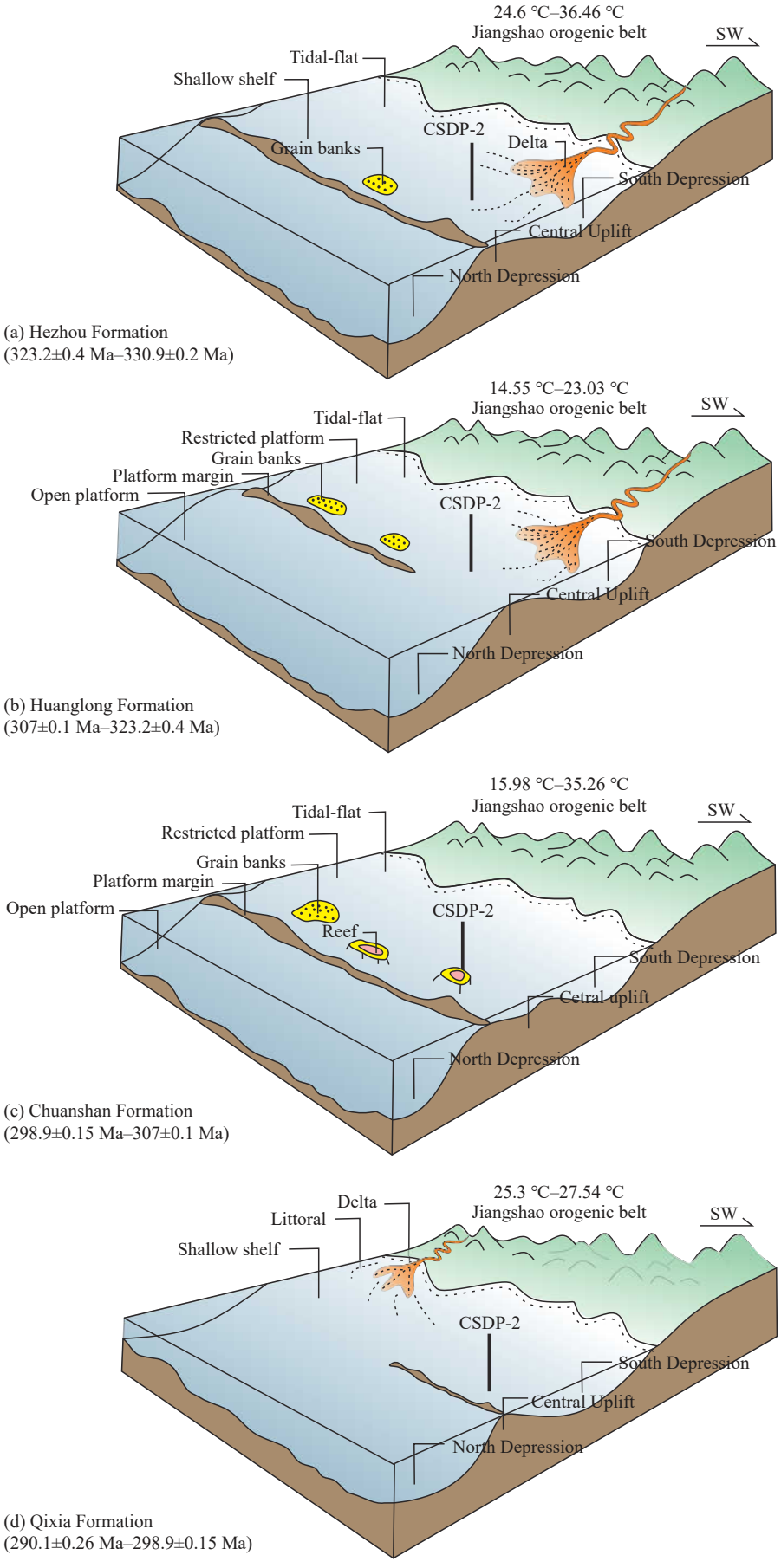

Fig. 10. Evolution of Carboniferous-Early Permian sedimentary.

limestone, including micritic limestone, sparite limestone, and bioclastic limestone, which is a set of black and grey

limestone during the last regression (Fig. 8). Two negative $\delta^{13}C$ excursions reflect two regressions and transgressions in this period, resulting the alternation of an open platform and restricted platform (Fig. 8; Zhao MY and Zheng YF, 2014). At the end of the Huanglong Formation, the regression and denudation of the Late Pennsylvanian subperiod continental uplift were capped by a karst weathering crust (Fig. 2a; Li SY et al., 2015). As a result, the Huanglong Formation and the overlying formation were in pseudo-conformity contact, which can also be observed in the Chaohu area (Lin CM et al., 2002; Gao XH et al., 2020). In the last regression, the ratio of $^{87}Sr/^{86}Sr$ was higher, indicating that more terrigenous organic matter was carried into the seawater (Fig. 8). This result may be due to the changes in ocean circulation associated with the closure of the western end of the Paleotethys during the formation of Pangaea (Vai GB, 2003; Li N et al., 2021). In the high-frequency oscillatory environment of the marine deposition, the paleo-highland was characterized by high wave agitation energy. The intergranular pores were well-developed due to the leaching and dissolution of the late atmospheric precipitation, leading to a higher porosity in the paleo-highland. In contrast, in the lowlands below the sea level, the tight lithology was deposited over time (Figs. 2o, p, q, r). These areas were less susceptible to dissolution by meteoric water, with low development of primary pore space (Fig. 6d).

During the Late Carboniferous Chuanshan period (from 298.9±0.15 Ma to 307±0.1 Ma), the weather was hot and humid (15.98°C–35.26°C), with seawater intrusion and migration of sediments to the southeast. The SYSB was in a restricted platform and tidal-flat environment from east to west, with organic reef shoal sub-facies developed in local highlands (Fig. 10c). In this period, a large amount of bioclastic limestone was deposited due to the low sea level (Figs. 2b, c, f). The primary sedimentary conditions were good and barely affected by diagenesis, with largely preserved primary sedimentary pores (Fig. 9). The reservoir was partially good in the highlands (Fig. 6d). The end of the Chuanshan period indicates that an anoxic event occurred during the Carboniferous-Permian transition as a result of increased temperatures (Fig. 8; Tabor NJ and Poulsen CJ, 2008).

The Asselian-Early Sakmarian environment of South China was a massive epicontinental sea, representing a regionally stable carbonate platform (Wang CS et al., 1999; Wang Y and Jin YG, 2000). In the Qixia period (from 290.1± 0.26 Ma to 298.9±0.15 Ma) with warm weather (25.3°C to 27.54°C), the SYSB was in a paralic sedimentary (Fig. 10d), and the lithology was dominated by black mudstones and limestones (Fig. 2a and Fig. 8). The Early Permian was the largest transgression period in this area (Ross CA and Ross JRP, 1987, 1995), with the deposition of extensive bioclastic limestones rich in fusulinida, corals, foraminifera, and calcareous algae (Fig. 2a and Fig. 8). As a result, stable lithofacies and thick carbonate rocks were formed (Hu F, 2010). In the late Qixia period, the Lower Yangtze Plate began to retreat, and most of the Lower Yangtze region became deltas and lagoons-bay facies, indicating the end of the marine sedimentary history (Fig. 10d). With the regression of sea level, the reservoir of Qixia Formation exhibited limited development (Fig. 6d), and the large set of black mudstone mainly served as source rocks (Cai LX et al., 2021).

As mentioned above, the Central Uplift of SYSB was an inherited paleo-uplift from the Caledonian movement. During that time, it experiences a warm and humid tropical climate with abundant atmospheric precipitation. The favorable conditions for developing porous carbonate rocks are as follows. Firstly, shoal carbonate facies were mainly developed in the paleo-highland. The primary pores were intergranular pores, biologic cavities, and biologic skeleton pores formed in a high-energy environment. Secondly, dissolution occurred after the deposition of the shoal facies during the syngenetic or quasi-syngenetic period. The influence of meteoric water on the diagenetic process primarily occurred during the early diagenetic and epigenetic periods (terrestrial detrital and meteoric water in the syngenetic stage). The secondary pores that appeared after the exposure of highlights were mainly composed of dissolved pores, intergranular pores, and intragranular pores, which were more conducive to the preservation of pores.

5.2. Hydrocarbon potential discussion

According to fluid inclusion analysis, the Mesozoic-Paleozoic source rocks of the Lower Yangtze are good, and large-scale natural gas accumulated in the Ordovician and Silurian Formation (Chen JW et al., 2018; Zhang YG et al., 2018; Liang J et al., 2019). The lithology of the source rock is mainly black graptolite shales, with organic matter ranging from 1.0% to 4.0% and a predominance of type I and type II kerogen (Hu F et al., 2010). TOC content ranges from 1.2% to 4%. The content of (S_1+S_2) and the asphalt chloroform “A” is quite low in the source rock. The equivalent vitrinite reflectance ranges from 1.19% to 2.6%, with a high degree of thermal evolution. It belongs to the high mature/over-mature stage, characterized by dry gas and wet gas. In addition to burial, the high maturity in this region may be related to shallow lithospheric burial and large geothermal gradient, and extensive magmatism in the Meso-Cenozoic may also have a great influence.

Based on the biomarker analysis of saturated hydrocarbon and oil and gas inclusions analysis, the hydrocarbon sources in the Carboniferous-Lower Permian reservoir are mainly from the Late Ordovician Wufeng Formation and Lower Silurian Gaojiabian Formation, partly from the Lower Permian Qixia Formation (Zhang YG et al., 2018; Liang J et al., 2019). The source rocks of the Ordovician Wufeng Formation and Lower Silurian Gaojiabian Formation are of medium to high quality. The oil generation stage is mostly in the Late Devonian to Permian, while the peak of the gas generation is in the Late Triassic. The trap was mainly formed in the Indosinian period (T-J_2), with the oil generation stage preceding the trap formation. The gas generation peak of the source rock is well-matched with the formation time of the

trap. The generated gas migrated upward along the faults formed by the Indosinian movement and subsequently entered Carboniferous-Lower Permian carbonate reservoirs (Fig. 11). The Indosinian and Yanshanian movements caused the uplift and deformation of the formation, forming structural fractures and karst caves that enhance reservoir conditions. Meanwhile, the locally formed gas reservoir exhibits adjustment and reconstruction effects, representing a primary weak reconstruction-type model for reservoir formation. According to the lithology thickness statistics of borehole CSDP-2, the Upper Permian Longtan Formation shows thick mudstone with a cumulative thickness of 399 m and a displacement pressure of 18 Mpa–25 Mpa. Based on the seismic reflection, the Longtan Formation is characterized by parallel and continuous reflection, indicating that the cap rock is continuously distributed and relatively stable (Fig. 1d; Liang J et al., 2017). With Late Ordovician Wufeng Formation and Lower Silurian Gaojiabian Formation as source rocks, the Carboniferous-Lower Permian carbonate as the good reservoirs, Late Permian Longtan-Dalong Formation as the seal, the SYSB has a great potential for hydrocarbon accumulation.

6. Conclusions

(i) According to the petrophysical analysis, P-wave impedance is a sensitive elastic parameter that distinguishes bioclastic limestone from pure limestone and clastic rock. In addition, λρ is a physically sensitive elastic parameter, which decreases with increasing porosity;

(ii) The pre-stack simultaneous inversion method effectively predicts the porous carbonate reservoirs. The results show that the Carboniferous-Early Permian bioclastic limestone was well developed in the Central Uplift of the SYSB, such as the slope of the Hezhou Formation, paleo-highlands of the Huanglong Formation, and the Chuanshan Formation. Moreover, locally developed bioclastic limestone with 3%–5% porosities was also present in the Qixia Formation around the paleo-highland;

(iii) According to carbon, oxygen, and strontium isotope analysis, the Carboniferous-Early Permian period was characterized by a warm and humid tropical climate, abundant atmospheric precipitation, and alternating oxygen-rich and hypoxia. Four negative and positive $\delta^{13}C$ excursions occurred from the Hezhou Formation to the Huanglong Formation, indicating a long-time exposure of the carbonate formation and intense denudation. Terrigenous detrital was brought into the seawater in the early stage of the Hezhou Formation and the late stage of the Huanglong Formation, affecting the carbonate diagenesis.

(iv) The good physical properties (reservoirs) of porous carbonate in the study area are mainly related to the following factors: a) the Central Uplift was a succeeding paleo-uplift zone after the Caledonian movement, which formed a shoal facies in the paleo-highland; b) the carbonate formation was subjected to meteoric water leaching and dissolution during the syngenetic to quasi-syngenetic period due to fluctuations in the sea level. The secondary pores were enlarged, leading to the development of high-quality reservoirs in local formation. Therefore, leaching and dissolution during diagenesis are important factors for good reservoirs.

(v) Large-scale natural gas accumulation was developed in the Ordovician Wufeng Formation and Lower Silurian Formation, with source rocks in the high-mature/over-mature stage, characterized by dry gas and wet gas. With Late Ordovician Wufeng Formation and Lower Silurian Gaojiabian Formation as the high-mature/over-mature stage source rocks, the Carboniferious-Lower Permian carbonate as good reservoirs, and Late Permian Longtan-Dalong formation as the stable seal, the SYSB has a great potential for hydrocarbon accumulation.

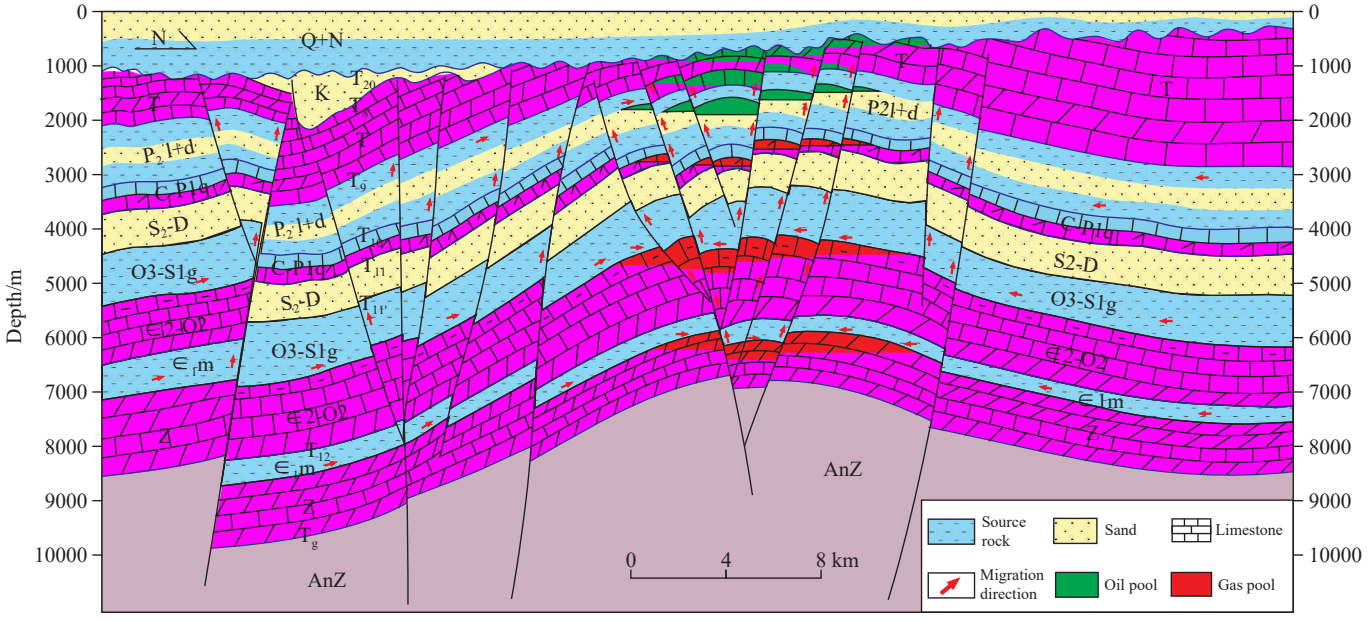

Fig. 11. Hydrocarbon migration path and accumulation model.

CRediT authorship contribution statement

Shu-yu Wu contributed to the presented idea and took the lead in writing the manuscript; Qi-liang Sun contributed to the supervision and writing of this work; Jian-wen Chen provided the original data; Jun Liu performed the analytic calculations. All authors discussed the results and contributed to the final manuscript.

Declaration of competing interest

The authors declare no conflicts of interest.

Acknowledgments

This study was supported by the project ofthe Science and Technology Innovation Fund of Command Center of Natural Resources Intergrated Survey entitled “Temporal and spatial distribution of paleochannel and origin of organic carbon burial in the Western Bohai Sea since 2.28Ma ” (KC20220011), the project entitled “Characterization of Carboniferous-Early Permian heterogeneous porous carbonate reservoirs and hydrocarbon potential analysis in the central uplift of the South Yellow Sea Basin”(KLSG2304) found by the Key laboratory of Submarine Science, Ministry of Natural Resources, the project entitled “1∶50000 Marine regional Geological survey in Caofeidian Sea Area, Bohai Sea ” (ZD20220602) , “1∶250000 Marine regional Geological survey in Weihai Sea Area, North Yellow Sea ” (DD20230412), and “Geological survey on tectonic and sedimentary conditions of Laoshan uplift ” (DD2016015) supported by the China Geological Survey, and the project entitled “Study on Hydrocarbon Accumulation Failure and Fluid Evolution Reduction of the Permian Reservoir in the Laoshan Uplift, South Yellow Sea” (42076220) organized by the National Natural Science Foundation of China. The authors would like to express their gratitude to the Qingdao Institute of Marine Geology, China Geological Survey for providing basic data and to Ph.D. Jian-wen Chen for his help in this study. The authors are also grateful to the editors and reviewers who provided sincere comments and assisted in writing this manuscript. The authors would like to thank KetengEdit (www.ketengedit.com) for its linguistic assistance during the preparation of this manuscript.

References

Armstrong-Altrin JS, Lee YI, Verma SP, Worden RH. 2009. Carbon, oxygen, and strontium isotope geochemistry of carbonate rocks of the Upper Miocene Kudankulam Formation, Southern India: Implications for paleoenvironment and diagenesis. Geochemistry, 69(1), 45–60. doi: 10.1016/j.chemer.2008.09.002.

Bao SH, Zhang XP, Yang YF, Guo XL. 2003. Gas potential identification of the oolitic beach reservoirs in Feixianguan formation in the North part of East Sichuan. Natural Gas Industry, 23(S1), 35–37 (in Chinese with English abstract).

Behrooz ED, Hossain RB. 2009. Effects of depositional and diagenetic characteristics on carbonate reservoir quality: A case study from the South Pars gas field in the Persian Gulf. Petroleum Geoscience, 15(4), 325–344. doi: 10.1144/1354-079309-817.

Bosence D. 2002. Carbonate reservoirs porosity evolution and diagenesis in a sequence stratigraphic framework. Marine And Petroleum Geology, 19(10), 1295–1296. doi: 10.1016/S0264-8172(03)00037-0.

Cai LX, Xiao GL, Guo XW, Wang J, Wu ZQ, Li BG. 2019. Assessment of Mesozoic and Upper Paleozoic source rocks in the South Yellow Sea Basin based on the continuous borehole CSDP-2. Marine and Petroleum Geology, 101, 30–42. doi: 10.1016/j.marpetgeo.2018.11.028.

Cai LX, Xiao GL, Zeng ZG, Zhang XH, Guo XW, Wang SP. 2020. New insights into marine hydrocarbon geological conditions in the South Yellow Sea Basin: evidence from borehole CSDP-2. Journal of Oceanology and Limnology, 38(4), 1169–1187. doi: 10.1007/s00343-020-0068-8.

Cai LX, Zhang XH, Guo XW, Zeng ZG, Xiao GL, Pang YM, Wang SP. 2021. Effective hydrocarbon-bearing geological conditions of the Permian strata in the South Yellow Sea Basin, China: Evidence from borehole CSDP-2. Journal of Petroleum Science and Engineering, 196, 1–21. doi: 10.1016/j.petrol.2020.107815.

Cao Q, Ye JR, Shi WZ. 2008. Application of the method of seismci attribution to prediction of source rock thickness in new exploration areas of North Depression in South Yellow Sea Basin. Marine Geology and Quaternary Geology, 28(5), 109–114 (in Chinese with English abstract).

Craig H. 1957. Isotopic standards for carbon and oxygen and correction factors for mass-spectrometric analysis of carbon dioxide. Geochimica et Cosmochimica Acta, 12(1), 133–149. doi: 10.1016/0016-7037(57)90024-8.

Chen HC, Wang YH, Yan YY. 1979. Early Carboniferous strata in the South of Jiangsu and Anhui. ACTA Stratigraphica Sinica, 3(4), 242–250.

Chen JW, Gong JM, Li G, Li HJ, Yuan Y, Zhang YX. 2016. Great resources potential of the marine Mesooic- Paleozoic in the South Yellow Sea Basin. Marine Geology Frontiers, 32(1), 1–7 (in Chinese with English abstract).

Chen JW, Liang J, Zhang YG, Yang CQ, Yuan Y, Xu M, Wang JQ, Lei BH, Li G, Yang YQ, Yang CS, Sun J. 2019. Regional evaluation of oil and gas resources in offshore china and exploration of oil and gas in the Yellow Sea and East China sea. Marine Geology and Quaternary Geology, 39(6), 1–29 (in Chinese with English abstract). doi: 10.16562/j.cnki.0256-1492.2019112001.

Chen JW, Xu M, Lei BH, Shi J, Liu J. 2020. Collision of North China Yangtze Plates: Evidence from the South Yellow Sea. Marine Geology and Quaternary Geology, 40(3), 1–12 (in Chinese with English abstract).

Chen JW, Zhang YG, Ou GX, Liang J, Yuan Y, Wu SY. 2018. The inclusion evidence of multi-phase hydrocarbon accumulation in the South Yellow sea. Marine Geology Frontiers, 34(2), 69–70 (in Chinese with English abstract).

Chen Y, Chen H, Guang D, Liu Y. 2013. The application of seismic technology in fluid discrimination of Carbonation reef oil and gas reservoir. Science Technology and Engineering, 13(21), 6208–6215 (in Chinese with English abstract).

Chen ZQ, Qu DP, Miao ZW. 2015. Seismic prediction of deep reef-bank reservoirs in the Changxing formation in the YB area. Development Application, 14(7), 20–26 (in Chinese with English abstract).

Clayton RN, Epstein S. 1958. Relationship between $^{18}O/^{16}O$ ratios in coexisting minerals of igneous and metamorphic rocks. Journal of Geology, 66(4), 345–371. doi: 10.1086/626523.

Dai SH, Tian B, Han YC. 2006. Prediction of matrix porous carbonate reservoir and application. OGP, 41(6), 681–686.

Du HK, Cai QX, Xiao B, Zheng L, Jin D, Xue YJ. 2017. Reservoir distribution prediction on the top of Middle Triassic Leikoupo formation in Puguang area. OGP, 52(6), 1269–1279 (in Chinese with English abstract).

Duan SM, Li YG, Pei JX, Zhao TH, Wu ZQ, Han B, Yu XS, Liu LJ, Chen JL, Xu ZH. 2020. Carbonate imaging with magnetotellurics in a shallow-water environment, South Yellow Sea, China. Journal of Applied Geophysics, 178, 104076 (in Chinese with English abstract). doi: 10.1016/j.jappgeo.2020.104076.

Feldman HR, Franseen EK, Joeckel RM, Heckel PH. 2005. Impact of Longer-Term Modest Climate Shifts on Architecture of High-

Frequency Sequences (Cyclothems), Pennsylvanian of Midcontinent U. S. A. Journal of Sedimentary Research, 75(3), 350–368. doi: 10.2110/jsr.2005.028.

Feng K, Chen ZQ, Zha CY. 2006. Carbonate complex lithological hydrocarbon reservoir forecast based on pre-stack seismic data-with gas reservoir in Feixianguan formation in East Sichuan as an example. Petroleum Geology and Development of Daqing, 25, 96–99 (in Chinese with English abstract).

Feng ZQ, Yao Y, Zeng XH, Wang Q, Wang LL, Chen Q, Yi H, Jin HF. 2002. New understanding of Mesozoic-Paleozoic tectonics and hydrocarbon potential in Yellow Sea. China Offshore Oil Gas, 16(6), 367–373 (in Chinese with English abstract).

Feng ZZ, He YB, Wu SH. 1993. Lithofacies paleography of Permian in Middle and Lower Yangtze region. ACTA Sedimentaologica Sinica, 11(3), 13–24 (in Chinese with English abstract).

Gao G. 2013a. Method for predicting th porosity based on the pore structure of carbonate. Progress in Geophysics, 28(2), 920–927 (in Chinese with English abstract).

Gao G, He ZH, Huang D, Gui Z, Wei W. 2013b. Research on predicting the porosity of carbonate reservoir in the Northeast area of Sichuan. Science Technology and Engineering, 13(10), 2635–2641 (in Chinese with English abstract).

Gao XH, Zhang XH, Guo XW, Cai LX, Hou FH, Zhu XQ. 2020. Provenance and Tectonic Implications of Paleozoic Strata in the South Yellow Sea Basin China–Revealed from the Borehole CSDP-2. Journal of Ocean University of China, 19(3), 536–550. doi: 10.1007/s11802-020-4088-y.

Guo TL. 2018a. Hydrocarbon accumulation conditions and key technologies for exploration and development of Yuanba gas field. Petroleum Research, 3(4), 293–305. doi: 10.1016/j.ptlrs.2018.11.004.

Guo XS, Hu, DF, Li YP, Duan JB, Ji CH, Duan H. 2018b. Discovery and theoretical and technical innovations of Yuanba gas field in Sichuan Basin, SW China. Petroleum Exploration and Development Online, 45(1), 15–28. doi: 10.1016/S1876-3804(18)30002-8.

Guo XW, Zhang XH, Wu ZQ, Xiao GL, Hou FH, Liu J. 2019. Scientific objective and preliminary progresses of CSDP-2 well in continental shelf drilling program. Journal of jilin university (Earth Science Edition), 49(1), 1–12 (in Chinese with English abstract).

He ZL, Wei XC, Qian YX, Bao ZM, Fan M, Jiao CL, Peng ST, Chen D. 2011. Forming mechanism and distribution prediction of quality marine carbonate reservoirs. Oil and Gas Geology, 32(4), 489–498 (in Chinese with English abstract).

Heckel PH. 1986. Sea-level curve for Pennsylvanian eustatic marine transgressive-regressive depositional cycles along midcontinent outcrop belt, North America. Geology, 14, 330–334.

Hu F. 2010. Hydrocarbon resources potential study in Mesozoic-Palaeozoic marine strata in the South Yellow Sea Bain. Offshore Oil, 30(3), 1–8 (in Chinese with English abstract).

Huang CS, Zhang JJ, Hu GC, Zhang LJ, Chen HB, Wei DY, Cai D, Yu YJ, Li X, Ding P, Li J. 2021. Characterization of the distribution, source, and potential ecological risk of perfluorinated alkyl substances (PFASs) in the inland river basin of Longgang District, South China. Environmental Pollution, 287, 117642. doi: 10.1016/j.envpol.2021.117642.

Huang HX, Deng Y, Wu ZP, He GM, Xiong Y, Liu HF. 2003. Application of absorption coefficient inversion in prediction of Carbonate reservoir in the East of Sichuan. Geophysical Prospecting for Petroleum, 42(1), 86–88 (in Chinese with English abstract).

Hong HL, Zhao H, Zhang LF, Jia ZH, Li QZ, Zhou TF. 2014. The Early Carboniferous zircon U-Pb chronology and its sedimentary significance in the northern Chaohu area, Anhui, East China. Acta Petrologica Sinica, 30(4), 1087–1096 (in Chinese with English abstract).

Ji XW, Zhang YQ, Zang DG, Sheng P, Feng XK, Xu B. 2012. Carbonate reef- shoal reservoir identification in Western Longgang, Sichuan Basin. OGP, 47(2), 309–314 (in Chinese with English abstract).

Jiang XD, Zhu SJ, Zhang GR, Zhang XL, Cao S. 2014. Reservoir prediction of Maokou formation, Southern Sichuan basin. Natural Gas Exploration and Development, 37(1), 37–40 (in Chinese with English abstract).

Jin XJ, Hou JG, Liu HL, Zhang JX, Liu H. 2016. Seismic prediction method of permeability of reef bank reef reservoir with complex pore types in Puguang gasfield. Journal of Palaeogeography, 18(2), 275–284 (in Chinese with English abstract).

Keith ML, Weber JN. 1964. Carbon and oxygen isotopic composition of selected limestones and fossils. Geochimica et Cosmochimica Acta, 28, 1787–1816. doi: 10.1016/0016-7037(64)90022-5.

Lécuyer C, Daux V, Moissette P, Cornée J, Quillévéré F, Koskeridou E, Fourel F, Martineau F, Reynard B. 2012. Stable carbon and oxygen isotope compositions of invertebrate carbonate shells and the reconstruction of paleotemperatures and paleosalinities-A case study of the early Pleistocene of Rhodes Greece. Palaeogeography, Palaeoclimatology, Palaeoecology, 350–352, 39–48. doi: 10.1016/j.palaeo.2012.06.009.

Lei BH, Xu M, Chen JW, Liang J, Zhang YG. 2018. Structural characteristics and evolution of the South Yellow Sea Basin since Indosinian. China Geology, 1(4), 466–476. doi: 10.31035/cg2018063.

Lei FL, He ZH, Wen XT, Xu P. 2010. Study on prediction method of porosity of carbonate reservoir in ZH area. Journal of Oil and Gas Technology, 32(3), 236–239.

Li JL, Chen ZQ, Wang LJ, Liu LH, Li JH. 2017. Application of facies-controlled technique to bioclastic shoal reservoir prediction in less well zones. Lithologic Reservoir, 29(3), 110–117 (in Chinese with English abstract).

Li RF, Liu BP, Zhao CL. 1997. Cycle-Sequences, Carbon Isotope Features and Glacio-Eustasy of the Triticites Zone in Southern Guizhou. Acta geologica Sinica (English Edition). 71(2), 217−226.

Li N, Wang C, Zong P, Mao Y. 2021. Coevolution of global brachiopod palaeobiogeography and tectonopalaeogeography during the Carboniferous. Journal of Palaeogeography, 1(10), 1–18. doi: 10.1186/s42501-021-00095-z.

Li SY, Jin FQ. 1994. Carboniferous paleography in the Lower Yangtze basin. Journal of Hefei University of Technology, 17(3), 167–174 (in Chinese with English abstract).

Li SY, Jiang D, Zhao YY, Hu XM, Shi YK. 2015. Carboniferous- Early Permian carbonate microfacies and sedimentay environments in the Chaohu region, Anhui. Sedimentary Geology and Tethyan Geology. 35(1), 3–15.

Li WY, Liu YX, Xu JC. 2014. Onshore–offshore structure and hydrocarbon potential of the South Yellow Sea. Journal of Asian Earth Sciences, 90, 127–136. doi: 10.1016/j.jseaes.2014.04.024.

Li Y, Kang ZJ, Xue ZJ, Zheng SQ. 2018. Theories and practices of carbonate reservoirs development in China. Petroleum Exploration and Development Online, 45(4), 712–722. doi: 10.1016/S1876-3804(18)30074-0.

Liang J, Zhang PH, Chen JW, Gong JM, Yuan Y. 2017. Hydrocarbon preservation conditions in Mesozoice-Paleozoic marine strata in the South Yellow Sea Basin. Natural Gas Industry B, 4, 432–441. doi: 10.1016/j.ngib.2017.05.013.

Liang J, Chen JW, Wang JQ, Zhang PH, Wu SY, Zhang YG, Xu M. 2019. Hydrocarbon geological conditions and exploration prospects of marine strata in the Laoshan Uplift, South Yellow Sea Basin. Acta Geologica Sinica (english edition), 93(supp.2), 303–304.

Liang J, Zhang YG, Dong G, Xiong BH. 2011. A discussion on marine Mesozoic- Palaeozoic reservoirs in south yellow sea. Marine Geology & Quaternary Geology. 31(5), 101−108. (in Chinese with English abstract).

Lin CM, Huang, ZC, Liu, JR, Ling, HF, Zhang, S, Zhao, YY, 2002. Carboniferous microfacies and sequence stratigraphy of Fenghuangshan profile in Chaohu of Anhui province, China. Acta Petrologica Sinica, 18(3), 424–433 (in Chinese with English abstract).

Liu GP, You YC, Feng Q, Wang D. 2017. Fine depict of reef reservoirs in Changxing formation, Yuanba area. OGP, 52(3), 583–590 (in Chinese with English abstract).

Liu J, Chen JW, Wu SY, Zhang YG, Shi J, Liu H, Yuan CF. 2018. Pre-stack three-term seismic inversion for prediction of Carboniferous-Lower Permian cabonate reservoir on the Central Uplift of South Yellow Sea basin. Marine Geology and Quaternary Geology 38(3),

186–198 (in Chinese with English abstract).
Liu XX, Yin XY, Zhang F. 2013. S-wave velocity estimation method in carbonate reservoir. Journal of China University of Petroleum, 37(1), 42–49 (in Chinese with English abstract).
Lu P, Luo P, Wei W, Zhu C. 2022. Effects of gas saturation and reservoir heterogeneity on thermochemical sulfate reduction reaction in a dolomite reservoir, Puguang gas field, China. Marine and Petroleum Geology, 135, 105402. doi: 10.1016/j.marpetgeo.2021.105402.
Luo P, Zhang JD, Liu W, Song JM, Zhou G, Sun P, Wang DC. 2008. Characteristic of marine carbonate hydrocarbon reservoirs in China. Earth Science Frontiers, 15(1), 36–50 (in Chinese with English abstract).
Lv QB, Wu QJ, Bi YY. 2012. Prediction of reef-flat reservoir using high resolution seismic interpretation. Xinjiang Petroleum Geology, 33(5), 557–559 (in Chinese with English abstract).
Ma LW, Gu HM, Zhao YY, Chen DY, Zhao XP. 2013. Sculpturing platform-edge reef carbonate reservoirs in deep-water with random media forward modeling. OGP, 48(4), 583–590 (in Chinese with English abstract).
Ma YS, Guo XS, Fang R. 2005. Reservoir prediction of Feixianguan formation in Puguang gas field, Northeast Sichuan Province. Petroleum Exploration and Development, 32(4), 60–64 (in Chinese with English abstract).
Ma YS, Cai XY, Zhao PR, Feng ZX. 2010. Formation mechanism of deep-buried carbonate reservoir and its model of three-element controlling reservoir: A case study from the Puguang oilfield in Sichuan. Acta Geologica Sinica, 84(8), 1087–1094 (in Chinese with English abstract).
Masoud SY, Hossain RB, Vahid T, Maziyar N, Mohammad KR. 2019. Linking diagenetic history to depositional attributes in a high-frequency sequence stratigraphic framework: A case from upper Jurassic Arab formation in the central Persian Gulf. Journal of African Earth Sciences, 153, 91–110. doi: 10.1016/j.jafrearsci.2019.02.006.
Mcelhinny MW. 1985. Permian paleomagnetism of the western yangtze block, China: A reinterpretation. Journal of Geodynamics, 2(2), 115–117.doi. doi: 10.1016/0264-3707(85)90004-3.
Muhammad ZAD, Maryam T, Anwar A, Bakhtawer S, Syed AR. 2021. Characterization of carbonate reservoir using post-stack global geostatistical acoustic inversion approach: A case study from a mature gas field, onshore Pakistan. Journal of Applied Geophysics, 188, 104313. doi: 10.1016/j.jappgeo.2021.104313.
Nooshafarin H, Hossein H, Vahid T, Galina PN. 2020. Permian–Triassic extinction pattern revealed by foraminifers and geochemical records in the central Persian Gulf, southern Iran. Palaeogeography, Palaeoclimatology, Palaeoecology, 543, 109588. doi: 10.1016/j.palaeo.2020.109588.
Pang YM, Guo XW, Chang XC, Zhang JJ, Zhou JQ, Cai LX. 2021. Characteristics and classification of paleozoic tight reservoirs in the central uplift of the South Yellow Sea Basin. Energy Geoscience, 3(4), 383–393. doi: 10.1016/j.engeos.2021.05.002.
Pekar SF, McHugh CMG, Christie-Blick N, Jones M, Carbotte SM, Bell RE, Lynch-Stieglitz J. 2004. Estuarine processes and their stratigraphic record: paleosalinity and sedimentation changes in the Hudson Estuary (North America). Marine Geology, 209, 113–129. doi: 10.1016/j.margeo.2004.05.025.
Qie WK, Zhang XH, Du YS, Zhang Y. 2011. Lower carboniferous carbon isotope stratigraphy in South China: Implications for the Late Paleozoic glaciation. Science China Earth Sciences, 54(1), 84–92. doi: 10.1007/s11430-010-4062-4.
Qin SF, Yang Y, Lv F, Zhou H, Li YX. 2016. The origin of gas in the Changxing–Feixianguan gas pools in the Longgang gas field in the Sichuan Basin, China. Journal of Natural Gas Geoscience, 1(5), 327–334. doi: 10.1016/j.jnggs.2016.11.002.
Ross CA, Ross JRP. 1987. Late Paleozoic sea levels and depositional sequences. Special Publications- Cushman Foundation for Foraminiferal Research, 24, 137–149.
Ross CA, Ross JRP. 1995. Late Paleozoic depositional sequences are synchronous and worldwide. Geology, 13, 194–197.
Sampei Y, Matsumoto E, Dettman DL, Tokuoka T, Abe O. 2005. Paleosalinity in a brackish lake during the Holocene based on stable oxygen and carbon isotopes of shell carbonate in Nakaumi Lagoon, southwest Japan. Palaeogeography, Palaeoclimatology, Palaeoecology 224(4), 352–366. doi: 10.1016/j.palaeo.2005.04.020.
Sheng QH, Zhang JM. 2016. Identification of fluid based on deconvolution short-time fourier transform- taking Yuanba area as an example. Science Technology and Engineering, 16(15), 41–46 (in Chinese with English abstract).
Sheng QY, Zheng QF, Wu XH, Zhang YQ, Wang XD. 2013. Biostratigraphic and sedimentological progress of the Carboniferous Hezhou Formation at Chaohu, Anhui province. Journal of Stratigraphy, 37(1), 41–47 (in Chinese with English abstract).
Shi GR, Chen ZQ. 2006. Lower Permian oncolites from South China: Implications for equatorial sea-level responses to late Palaeozoic Gondwanan glaciation. Journal of Asian earth sciences, 26(3−4), 424–436. doi: 10.1016/j.jseaes.2005.10.009.
Shinn YJ. 2015. Geological structures and controls on half-graben inversion in the western Gunsan Basin, Yellow Sea. Marine and Petroleum Geology, 68, 480–491. doi: 10.1016/j.marpetgeo.2015.09.013.
Shinn YJ, Chough SK, Hwang IG. 2010. Structural development and tectonic evolution of Gunsan Basin (Cretaceous–Tertiary) in the central Yellow Sea. Marine and Petroleum Geology, 27(2), 500–514. doi: 10.1016/j.marpetgeo.2009.11.001.
Smith JLB, Read JF. 2000. Rapid onset of late Paleozoic glaciation on Gondwana: Evidence from Upper Mississippian strata of the Midcontinent, United States. Geology, 28, 279–282.
Tabor NJ, Poulsen CJ. 2008. Palaeoclimate across the Late Pennsylvanian–Early Permian tropical palaeolatitudes: A review of climate indicators their distribution, and relation to palaeophysiographic climate factors. Palaeogeography, Palaeoclimatology, Palaeoecology, 268, 293–310. doi: 10.1016/j.palaeo.2008.03.052.
Tong J, Zhang XJ, Zhang W, Xiong SQ. 2018. Marine strata morphology of the South Yellow Sea based on high-resolution aeromagnetic and airborne gravity data. Marine and Petroleum Geology, 96, 429–440. doi: 10.1016/j.marpetgeo.2018.06.018.
Vai GB. 2003. Development of the palaeogeography of Pangaea from Late Carboniferous to Early Permian. Palaeogeography, Palaeoclimatology, Palaeoecology 196, 125–155. doi: 10.1016/S0031-0182(03)00316-X.
Veevers JJ, Powell CM. 1987. Late Paleozoic glacial episodes in Gondwanaland reflected in transgressive-regressive depositional sequences in Euramerica. Geological Society of America Bulletin, 98, 475–487. doi: 10.1130/0016-7606(1987)98<475:LPGEIG>2.0.CO;2.
Wang CS, Li, XH, Chen, HD, Tan, JX., 1999. Permian sea- level changes and rising- falling events in South China. ACTA Sedimentologica Sinica, 17(4), 39–44 (in Chinese with English abstract).
Wang H, Ma RH, Chen ZQ, Jian GM. 2019. Fine characterization of reefs and reservoir prediction of changxing formation in Yuanba gas field of Northeastern Sichuan Basin. Journal of Yangtze University (Natural Science Edition), 16(2), 21–26+5 (in Chinese with English abstract).
Wang JQ, Chen JW, Liang J, Sun J. 2016. Application of spectrum decomposition to tthe laoshan uplift, South Yellow Sea. Marine Geology Frontiers, 32(10), 38–43 (in Chinese with English abstract).
Wang QC, Li R, Pu PW, Wang SJ. 2008. Study on seismic identification of organic reef distribution in Changxing formation, Northeast Sichuan. Geophysical and Geochemical Computing Techniques, 30(4), 282–287 (in Chinese).
Wang QT, Wang TL, Liu WP, Zhang J, Feng Q, Lu H, Peng PA. 2019. Relationships among composition, porosity and permeability of Longmaxi Shale reservoir in the Weiyuan Block, Sichuan Basin, China. Marine and Petroleum Geology, 102, 33–47. doi: 10.1016/j.marpetgeo.2018.12.026.
Wang W, Hu MY, Hu ZG, Yang W, Li YF, Dai L. 2013. Inter-well connectivity types analysis of fracture-cavity carbonate reservoir at block 6 in the Tahe oil fields. Science Technology and Engineering,

13(34), 10272–10278 (in Chinese with English abstract).
Wang XD, Hu KY, Qie WK, Sheng QY, Chen B, Lin W, Yao L, Wang QL, Qi YP, Chen JT, Liao ZT, Song JJ. 2019. Carboniferous integrative stratigraphy and timescale of China. Science China Earth Sciences, 62(1), 135–153. doi: 10.1007/s11430-017-9253-7.
Wang Y, Jin YG. 2000. Permian Palaeogeographic Evolution of the Jiangnan Basin, South China. Palaeogeography, Palaeoclimatology, Palaeoecology, 160(1−2), 35–44. doi: 10.1016/S0031-0182(00)00043-2.
Wennberg O, Casini G, Jonoud S, Peacock D. 2016. The characteristics of open fractures in carbonate reservoirs and their impact on fluid flow: A discussion. Petroleum Geoscience, 22(1), 91–104. doi: 10.1144/petgeo2015-003.
Wei GQ, Chen GS, Du SM, Zhang L, Yang W. 2008. Petroleum systems of the oldest gas field in China: Neoproterozoic gas pools in the Weiyuan gas field, Sichuan Basin. Marine and Petroleum Geology, 25, 371–386. doi: 10.1016/j.marpetgeo.2008.01.009.
Wu SY, Chen JW, Liang J, Liu J, Zhang YG, Yuan Y. 2016a. Characteristics of Mesozoic-Palaeozoic marine carbonate reservoir in the South Yellow Sea basin and hydrocarbon accumulation: comparison between the Sichuan Basin and the Subei basin. Marine Geology Frontiers, 32(1), 13–21 (in Chinese with English abstract).
Wu SY, Chen JW, Liu J, Zhang YG, Liang J, Yuan Y, Tao R. 2016b. Application of s-wave well logging predicted for pre-stack inversion in the South Yellow Sea basin. Marine Geology Frontiers, 32(10), 51–59 (in Chinese with English abstract).
Wu SY, Liu J, Chen JW, Yuan Y, Liang J, Zhang YG, Shi J. 2019. Pre-stack simultaneous inversion in the marine carbonate reservoir prediction of the South Yellow Sea Basin, China. Acta geologica Sinica (English Edition), 93(supp.2), 420–421.
Wu SY, Liu J, Xiao GL, Zhang YG, Zhao TH. 2011. Application of seismic attribute analysis to The Permian-Triassic deposits in the South Yellow Sea. Marine Geology and Quaternary Geology, 31(5), 109–116 (in Chinese with English abstract). doi: 10.3724/SP.J.1140.2011.05109.
Wu YW, Tian H, Li TF, Ji S, Liu ZY, Xiao XM, Xie LH. 2021. Enhanced terrestrial organic matter burial in the marine shales of Yangtze platform during the early Carboniferous interglacial interval. Marine and Petroleum Geology, 129, 105064. doi: 10.1016/j.marpetgeo.2021.105064.
Xie F, Li ZR, Xiao FS, Deng Y, He C. 2004. Prediction technique for the oolitic beach reservoir of Feixianguan formation in the Northeast of Sichuan basin by using seismic data. Natural Gas Industry, 24, 34–36 (in Chinese with English abstract).
Xu M, Chen JW, Liang, J, Zhang YG, Lei BH, Shi J, Wang JQ, Liu J, Liu H. 2019. Basement structures underneath the northern South Yellow Sea basin (East China): Implications for the collision between the North China and South China blocks. Journal of Asian Earth Sciences, 186, 104040. doi: 10.1016/j.jseaes.2019.104040.
Yang Y, Xie JR, Zhao LZ, Huang PH, Zhang XH, Chen C, Zhang BJ, Wen L, Wang H, Gao ZL, Shan SJ. 2021. Breakthrough of natural gas exploration in the beach facies porous dolomite reservoir of Middle Permian Maokou Formation in the Sichuan Basin and its implications: A case study of the tridimensional exploration of Well JT1 in the central-northern Sichuan Basin. Natural Gas Industry B, 8(4), 393–401. doi: 10.1016/j.ngib.2021.07.010.
Yang ZC, Gao LJ, Li HY. 2017. Match pursuit time-frequency analysis technology in the prediction of fractured reservoir in Tahe oilfield. Geological Science and Technology Information, 36(3), 293–298 (in Chinese with English abstract).
Yao YJ, Chen CF, Feng ZQ, Ying ZS, Hao TY, Wan RS. 2010. Tectonic evolution and hydrocarbon potential in northern area of the South Yellow Sea. Journal of Earth Science, 21(1), 71–82 (in Chinese with English abstract). doi: 10.1007/s12583-010-0006-3.
Yuan Y, Chen JW, Liang J, Zhang PH, Wu SY, Zhang YG. 2016. Discussion on exploration targets of marine Mesozoic and Paleozoic hydrocarbon in the South Yellow Sea. Marine Geology Frontiers, 32(10), 44–50 (in Chinese with English abstract).
Zhang GR, Zhang X, Yu Y, Zhang HY, Liao Q, Zhang HF, Zhao AL, Liang H. 2017. Key techniques for prediction of fractured carbonate reservoirs in deep marine carbonate rocks in Sichuan basin: A case study of the Maokou formation in SN area. Natural Gas Geoscience, 28(8), 1235–1242 (in Chinese with English abstract).
Zhang XF. 2011. Special elemental sulfur in the dolomite reservoirs of the giant Puguang Gas Field: Proof of crude oil involved thermochemical sulfate reduction. Procedia Earth and Planetary Science, 2, 229–234. doi: 10.1016/j.proeps.2011.09.037.
Zhang XH, Guo XW, Wu ZQ, Xiao GL, Zhang XH, Zhu XQ. 2019. Preliminary results and geological significance of well CSDP-2 in the Central Uplift of South Yellow Sea basin. Chinese Journal Geophysics, 62(1), 197–218 (in Chinese with English abstract).
Zhang XH, Wu ZQ, Sun YB, Guo XW. 2017. Application of spectral decomposition to detect Mesozoic- Paleozoic reservoir on the Central of the South Yellow Sea basin. Oceanologica Sinica, 39(7), 102–109 (in Chinese with English abstract).
Zhang YG, Chen JW, Liang J, Ou GX, Wu D. 2018. Evidence of the existence of paleo reservoirs in Laoshan Uplift of the South Yellow Sea Basin. China Geology, 1(4), 566–567. doi: 10.31035/cg2018067.
Zhang YG, Chen JW, Wu SY, Yuan CF, Zhao YH. 2016. Reservoir prediction for deposits from Hezhou formation of Lower Carboniferous to Qixia formation of Lower Permian on the Laoshan Uplift of the South Yellow Sea. Marine Geology Frontiers. 32(10), 60-64. (in Chinese with English abstract).
Zhao MY and Zheng YF. 2014. Marine carbonate records of terrigenous input into Paleotethyan seawater: Geochemical constraints from Carboniferous limestones. Geochimica et Cosmochimica Acta, 141, 508–531 (in Chinese with English abstract). doi: 10.1016/j.gca.2014.07.001.
Zhao SJ, Li SZ, Suo YH, Guo LL, Dai LM, Jiang SH, Wang G. 2017. Structure and formation mechanism of the Yellow Sea Basin. Earth Science Frontiers, 24(4), 239–248 (in Chinese with English abstract).
Zhao WZ, Hu SY, Liu W, Wang TS, Li YX., 2014. Petroleum geological features and exploration prospect in deep marine carbonate strata onshore China: A further discussion. Natural Gas Industry, 34(4), 1–9 (in Chinese with English abstract).
Zhao WZ, Hu SY, Xu ZH, Zeng HL, Liu W, Fu QL, Shi SY, Wang L, Jiang L. 2018. Lithology mapping of a mixed siliciclastic-carbonate-evaporite system using 3D seismic and well data: Lower Triassic Jialingjiang Formation, Sichuan Basin, southwestern China. Marine and Petroleum Geology, 93, 422–436. doi: 10.1016/j.marpetgeo.2018.03.005.
Zhao WZ, Wang ZC, Jiang H, Fu XD, Xie WR, Xu AN, Shen AJ, Shi SY, Huang SP, Jiang QC. 2020. Exploration status of the deep Sinian strata in the Sichuan Basin: Formation conditions of old giant carbonate oil/gas fields. Natural Gas Industry B, 7, 462–472. doi: 10.1016/j.ngib.2020.09.004.
Zhou Q, Xiao XM, Tian H, Pan L. 2014. Modeling free gas content of the Lower Paleozoic shales in the Weiyuan area of the Sichuan Basin, China. Marine and Petroleum Geology, 56, 87–96. doi: 10.1016/j.marpetgeo.2014.04.001.
Zou CN, Du JH, Xu CC, Wang ZC, Zhang BM, Wei GQ, Wang TS, Yao G, Deng SW, Liu JJ, Zhou H, Xu AN, Yang Z, Jiang H, Gu ZD. 2014. Formation, distribution, resource potential and discovery of the Sinian-Cambiran giant gas field, Sichuan Basin, SW China. Petroleum Exploration and Development, 41(3), 278–293 (in Chinese with English abstract).
Zhu WL, Wu JF, Zhang GC, Ren JY, Zhao ZG, Wu KQ, Zhong K, Liu SX. 2015. Discrepancy tectonic evolution and petreleum exploration in China offshore Cenozoic basins. Earth Science Frontiers, 22(1), 88–101 (in Chinese with English abstract).
Zhu WL, Chen CF, Zhang BC, Wan YZ, Fu XW, Zhang YG. 2020. Paleozoic basin prototype evolution and source rock development in the South Yellow Sea. Petruleum Geology and Experiment, 42(5), 728–741 (in Chinese with English abstract).